symmetry

IMPACT FACTOR 2.940

CITESCORE 4.3

Article

Fully Heavy Tetraquark Spectroscopy in the Relativistic Quark Model

Rudolf N. Faustov, Vladimir O. Galkin and Elena M. Savchenko

Special Issue

Tetra- and Pentaquarks “Phenomenology of Multiquark States: Is There Approximate Symmetry between Diquarks and Antiquarks?”

Edited by
Dr. Alexandr Berezhnoy

MDPI

https://doi.org/10.3390/sym14122504

symmetry

MDPI

Article

Fully Heavy Tetraquark Spectroscopy in the Relativistic Quark Model

Rudolf N. Faustov [1], Vladimir O. Galkin [1] and Elena M. Savchenko [1,2,*]

[1] Federal Research Center "Computer Science and Control", Russian Academy of Sciences, Vavilov Street 40, 119333 Moscow, Russia
[2] Faculty of Physics, M. V. Lomonosov Moscow State University, Leninskie Gory 1-2, 119991 Moscow, Russia
* Correspondence: savchenko.em16@physics.msu.ru

Abstract: Masses of the ground and excited (1P, 2S, 1D, 2P, 3S) states of the fully heavy tetraquarks, composed of charm (c) and bottom (b) quarks and antiquarks, are calculated in the diquark–antidiquark picture within the relativistic quark model based on the quasipotential approach and quantum chromodynamics. The quasipotentials of the quark–quark and diquark–antidiquark interactions are constructed similarly to the previous consideration of mesons and baryons. Relativistic effects are consistently taken into account. A tetraquark is considered a bound state of a diquark and an antidiquark. The finite size of the diquark is taken into account, using the form factors of the diquark–gluon interaction. It is shown that most of the investigated states of tetraquarks lie above the decay thresholds into a meson pair; as a result, they can be observed only as broad resonances. The narrow state X(6900) recently discovered in the di-J/ψ production spectrum by the LHCb, CMS and ATLAS Collaborations corresponds to an excited state of the fully charmed tetraquark. Other recently discovered exotic heavy resonances, X(6200), X(6400), X(6600), X(7200), and X(7300), can also be interpreted as the different excitations of the fully charmed tetraquark.

Keywords: tetraquark; diquark; heavy quark; relativistic quark model

Citation: Faustov, R.N.; Galkin, V.O.; Savchenko, E.M. Fully Heavy Tetraquark Spectroscopy in the Relativistic Quark Model. *Symmetry* **2022**, *14*, 2504. https://doi.org/10.3390/sym14122504

Academic Editor: Jorge Segovia

Received: 28 October 2022
Accepted: 22 November 2022
Published: 26 November 2022

1. Introduction

The quark model of hadrons predicts various possible stable combinations of valence quarks and antiquarks, but for many decades, only two kinds of combinations were observed: baryons, consisting of three quarks (qqq), and mesons, consisting of a quark and an antiquark ($q\bar{q}$). Other possible combinations, such as tetraquarks ($qq\bar{q}\bar{q}$), pentaquarks ($qqqq\bar{q}$), glueballs (gg), hybrids ($q\bar{q}g$) and others, were called "exotic".

For many years, the very existence of those states was unclear since there was no convincing experimental evidence for them. The first reliable candidate for an exotic state was the X(3872) particle (Belle 2003 [1]). This is a charmonium-like state with an extremely narrow width ($\Gamma = 1.19 \pm 0.21$ Mev [2]) and uncharacteristic decays breaking the isospin ($\frac{Br(X(3872)\to\omega J/\psi)}{Br(X(3872)\to\pi^+\pi^- J/\psi)} = 1.1 \pm 0.4$ [1,3]). Thus, the X(3872) does not fit into the naive quark picture of hadrons except when in the form of the two-quark–two-antiquark state ($cu\bar{c}\bar{u}$). Soon after, the first explicitly exotic state $Z_c^{\pm}(4430)$ (LHCb 2014 [4]) was discovered. This particle is of special interest since it is the charged charmonium state. A nonzero electric charge means that, in addition to a pair of charmed quark and antiquark, it contains also a light quark and antiquark of different flavors ($cu\bar{c}\bar{d}$, $cd\bar{c}\bar{u}$). Currently a few dozen of candidates and reliably confirmed tetraquarks ($cc\bar{c}\bar{c}$ — X(6900) – LHCb 2020 [5], CMS 2022 [6], ATLAS 2022 [7], etc.) and pentaquarks ($uudc\bar{c}$ – $P_c^+(4380)$, $P_c^+(4450)$ – LHCb 2015 [8]) have been discovered. The most recent detailed review can be found in Ref. [9].

The unified theoretical picture of exotic states has not been developed yet. In the absence of a direct description of hadrons from first principles of QCD, theorists have to use model assumptions about the structure and nature of the interaction of quarks in exotic

hadrons. As a result, there are theoretical approaches that assume a different composition of exotic states and methods for their nonperturbative description. The predictions obtained within their framework agree with experimental data with varying degrees of success. The object of our research from all exotic states is fully heavy tetraquarks, consisting of two heavy quarks and two heavy antiquarks. This choice significantly reduces the number of approaches applicable for their description. At the moment, there are already a number of theoretical calculations within the framework of different models, but there is no consensus on which of the predicted states are long-living enough for their experimental detection.

Experimental searches for such states are actively conducted at Large Hadron Collider (LHC) in CERN. At present, the LHCb [5,10], CMS [6,11,12] and ATLAS [7] Collaborations are actively searching for fully charmed $cc\bar{c}\bar{c}$ and fully bottom $bb\bar{b}\bar{b}$ tetraquarks. The fully charmed states $cc\bar{c}\bar{c}$ are searched as the intermediate resonances in the processes $p+p \to J/\psi(1S)J/\psi(1S)$, $p+p \to J/\psi(1S)\psi(2S)$and $p+p \to J/\psi\mu^+\mu^-$ at $\sqrt{s} = 7, 8$ and 13 TeV (LHCb). The predicted mass of the $cc\bar{c}\bar{c}$ tetraquark lies in the range of $5.8-7.4$ GeV. Searches for it were performed in the mass range $6.2-7.4$ GeV. In 2020, the LHCb Collaboration announced the discovery of the narrow resonance X(6900) in the di-J/ψ spectrum [5], which, according to the measured mass and width, is a candidate for the excited $cc\bar{c}\bar{c}$ state. Additionally, several other broad structures peaking at about 6.4 and 7.2 GeV were reported. They can be other excitations of the same $cc\bar{c}\bar{c}$ tetraquark. Later in 2022, CMS [6] and ATLAS [7] Collaborations presented preliminary data confirming X(6900) and giving hints of a few more states including structures at 6.4 and 7.2 GeV.

In the sector of fully bottom tetraquarks $bb\bar{b}\bar{b}$, there has been no progress yet. These tetraquark states are searched as the intermediate resonances in the processes $p+p \to \Upsilon(1S)\Upsilon(1S)$ and $p+p \to \Upsilon\mu^+\mu^-$ at $\sqrt{s} = 7, 8$ and 13 TeV (LHCb) and 8 and 13 TeV (CMS). The predicted mass of the $bb\bar{b}\bar{b}$ state lies in the range of $18.4-18.8$ GeV. Searches for the $bb\bar{b}\bar{b}$ state were carried out in the mass range of $17.5-20.0$ GeV (LHCb) [10], and $17.5-19.5$ GeV (CMS) [11,12]. CMS also searched for the narrow resonances in the mass range $16.5-27$ GeV. However, none of these studies revealed reliable signs of a resonance with properties expected for the exotic $bb\bar{b}\bar{b}$ state in the given process and at such energies.

The paper is organized as follows. In Section 2, we give a description and physical justification of the model for studying these tetraquark structures. In Section 3, we describe the relativistic quark model and its application to the calculation of the tetraquark mass spectra. In Section 4, we present the results of our calculations. In Section 5, we analyze our predictions, comparing them with the thresholds for the strong fall-apart decays. In Section 6, we give a comparison of our results with the predictions of other scientific groups. Finally, in Section 7, the results and conclusions are summarized.

2. Model Description of Fully Heavy Tetraquarks

Tetraquark is a bound state of two quarks and two antiquarks. There are six flavors of quarks, and according to their masses, they can be divided into two groups: light (with the current masses less than the $\Lambda_{\rm QCD} \approx 200$ MeV, quark confinement energy) and heavy (with masses larger than $\Lambda_{\rm QCD}$) quarks. Light quarks are the u-quark with mass $2.16^{+0.49}_{-0.26}$ MeV, d-quark with mass $4.67^{+0.48}_{-0.17}$ MeV and s-quark with mass $93.4^{+8.6}_{-3.4}$ MeV. Heavy quarks are the c-quark with mass 1.27 ± 0.02 GeV, b-quark with mass $4.18^{+0.03}_{-0.02}$ GeV and t-quark with mass 172.69 ± 0.30 GeV [2]. We will focus on the fully heavy tetraquarks. However, the t-quark is special. It is almost two orders of magnitude heavier than other heavy quarks, and thus, it quickly decays via the weak interaction, not having enough time to form a bound state [13]. Therefore, we will not consider it.

From the two flavors of quarks and antiquarks, many combinations can be made. We have already performed calculations for the ground states masses for all possible compositions [14,15]. However, given the large number of possible excited states, it is more rational to select and study those combinations that are easier to detect experimentally. The most convenient of these are the symmetric compositions: fully charmed $cc\bar{c}\bar{c}$, doubly

charmed bottom $cb\bar{c}\bar{b}$, and fully bottom $bb\bar{b}\bar{b}$ tetraquarks. The reason for the preference of such combinations is that the tetraquarks are formed from the closely produced quark and antiquark pairs. Thus, the formation of these states requires the production of only two pairs ($2 \times c\bar{c}$, $c\bar{c} + b\bar{b}$ and $2 \times b\bar{b}$), while the formation of other combinations requires the production of at least three pairs, which is a less probable event.

We consider the tetraquark as a bound state of a diquark QQ' and an antidiquark $\bar{Q}\bar{Q}'$. This model is not new and is widely used in the hadron spectroscopy, giving good agreement between the calculations (for example, baryon masses) and experiments. Additionally, the theoretically predicted spectrum of possible baryon excitations in the genuine three-body picture is much wider than the experimentally observed one. The quark–diquark model of baryons, on the other hand, freezes some degrees of freedom and imposes the necessary restrictions that bring the theory into better agreement with the experiment [16,17].

Another widely used model for the tetraquarks description is a molecular picture. We consider such a picture of fully heavy tetraquarks to be significantly less probable. Indeed, in this case, the meson molecule model has the following main problems. The interaction between mesons in a molecule is either due to the van der Waals forces, or through the exchange of another meson containing the same quarks as in the molecule. The van der Waals forces are weak in general and cannot provide sufficient binding. In the fully heavy tetraquarks, only heavy mesons can be exchanged: $c\bar{c}, c\bar{b}, b\bar{c}, b\bar{b}$. Such an interaction is described by the Yukawa potential, and its strength decreases with the increasing mass of the exchanged meson. Therefore, such a potential can provide a weak coupling in the case of the exchange of the light mesons, such as pions ($M_{\pi^\pm} = 139.57$ MeV [2]), but in the considered case ($M_{min} = M_{\eta_c} = 2983.9 \pm 0.4$ MeV [2]), the coupling will be vanishingly small.

In the diquark consideration, one must take into account that a (anti)diquark is a bound system of fermions, and therefore must obey the generalized Pauli principle: the complete wave function of a (anti)diquark must be antisymmetric. The diquark color representation can be either antitriplet (the antisymmetric color wave function) or sextet (the symmetric color wave function). However, in the case of sextet, the interaction potential between the quarks within the diquark is repulsive because the mean value of the product of the color SU(3) generators between sextet states is positive. Thus the corresponding diquark cannot be a bound state, which we consider inappropriate for our problem. The above argument applies to the antidiquark. In the following, we consider only color antitriplet diquarks. This means that if a (anti)diquark is composed of (anti)quarks of the same flavor (the symmetric flavor wave function), it can only have the symmetric spin wave function, thus being in the axialvector (A) state. If a diquark consists of quarks of different flavors, it can be either in the axialvector (A) or scalar (S) state.

3. Relativistic Diquark–Antidiquark Model

For the calculation of the masses of tetraquarks, we use the relativistic quark model based on the quasipotential approach and the diquark–antidiquark picture of tetraquarks. In this approach, the masses of tetraquarks are the solutions of the relativistic Schrödinger-type quasipotential equation [18–20]. This equation describes the bound state of two particles in a given quasipotential. We first apply it to the quark–quark system, forming a diquark and then to the diquark–antidiquark system forming a tetraquark [21,22]:

$$\left(\frac{b^2(M)}{2\mu_R(M)} - \frac{\mathbf{p}^2}{2\mu_R(M)}\right)\Psi_{T,d}(\mathbf{p}) = \int \frac{d^3q}{(2\pi)^3} V(\mathbf{p},\mathbf{q};M)\Psi_{T,d}(\mathbf{q}). \quad (1)$$

Here, $\mathbf{p}$ is a vector of the relative momentum, M is the mass of the bound state, and μ_R is the relativistic reduced mass of the constituents given by

$$\mu_R = \frac{E_1 E_2}{E_1 + E_2} = \frac{M^4 - (m_1^2 - m_2^2)^2}{4M^3}, \quad (2)$$

where $m_{1,2}$ are masses of the constituents and $E_{1,2}$ are the on-mass-shell energies of the constituents:

$$E_{1,2} = \frac{M^2 - m_{2,1}^2 + m_{1,2}^2}{2M}. \tag{3}$$

$b^2(M)$ is the on-mass-shell relative momentum in the center-of-mass system squared:

$$b^2(M) = \frac{[M^2 - (m_1 + m_2)^2][M^2 - (m_1 - m_2)^2]}{4M^2}, \tag{4}$$

$\Psi_{T,d}(\mathbf{p})$ are the bound state wave functions, and $V(\mathbf{p}, \mathbf{q}; M)$ is the quasipotential operator of the constituents.

Equation (1) is relativistic. On the left-hand side, it contains relativistic kinematics: the reduced mass of the bound state μ_R and the on-mass-shell relative momentum $b^2(M)$ are functions of the bound state mass M (Equation (2)). The relativistic dynamics is contained on the right-hand side of the Equation (1), in the quasipotential $V(\mathbf{p}, \mathbf{q}; M)$. The quasipotential is constructed with the help of the off-mass-shell scattering amplitude, projected onto the positive-energy states, and contains all relativistic spin-independent and spin-dependent contributions.

Constructing the quasipotential of the quark–quark interaction, we assume that the effective interaction is the sum of the usual one-gluon exchange term with the mixture of the long-range vector and scalar linear confining potentials, where the vector confining potential vertex contains the additional Pauli term. Due to the difference in the QQ' and $\bar{Q}\bar{Q}'$ color states, the quark–quark interaction quasipotential is considered to be $V_{QQ'} = \frac{1}{2}V_{\bar{Q}\bar{Q}'}$ of the quark–antiquark interaction quasipotential [16] and is given by

$$V(\mathbf{p}, \mathbf{q}; M) = \overline{u}_1(p)\overline{u}_2(-p)\mathcal{V}(\mathbf{p}, \mathbf{q}; M)u_1(q)u_2(-q), \tag{5}$$

with

$$\begin{aligned}\mathcal{V}(\mathbf{p}, \mathbf{q}; M) &= \mathcal{V}_{\mathrm{OGE}} + \mathcal{V}^V_{\mathrm{conf.}} + \mathcal{V}^S_{\mathrm{conf.}} \\ &= \frac{1}{2}\Bigg[\underbrace{\frac{4}{3}\alpha_s D_{\mu\nu}(\mathbf{k})\gamma_1^\mu\gamma_2^\nu}_{\mathrm{one-gluon-exchange}} + \underbrace{V^V_{\mathrm{conf.}}(\mathbf{k})\Gamma_1^\mu(\mathbf{k})\Gamma_{2;\mu}(-\mathbf{k}) + V^S_{\mathrm{conf.}}(\mathbf{k})}_{\mathrm{confinement}}\Bigg].\end{aligned} \tag{6}$$

Here $\mathbf{k} = \mathbf{p} - \mathbf{q}$, $\gamma_l^{\mu,\nu}$ and $u_l^\lambda(p)$ are the Dirac matrices and spinors:

$$u_l^\lambda(p) = \sqrt{\frac{\varepsilon_l(p) + m_l}{2\varepsilon_l(p)}}\begin{pmatrix} 1 \\ \frac{\sigma\mathbf{p}}{\varepsilon_l(p)+m_l}\end{pmatrix}\chi^\lambda, \quad l = 1, 2, \tag{7}$$

where $\varepsilon_l(p)$ is the quark energy:

$$\varepsilon_l(p) = \sqrt{m_l^2 + \mathbf{p}^2}, \quad l = 1, 2, \tag{8}$$

σ and χ^λ are the Pauli matrices and spinors:

$$\chi^\lambda = \begin{pmatrix}1\\0\end{pmatrix}, \begin{pmatrix}0\\1\end{pmatrix}, \quad \lambda = 1, 2. \tag{9}$$

α_s is the running QCD coupling constant with freezing [23,24]:

$$\alpha_s(\mu^2) = \frac{4\pi}{(11 - \frac{2}{3}\eta_f)\ln[\frac{\mu^2 + M^2_{BG}}{\Lambda^2}]}, \tag{10}$$

with

$$\begin{cases} \mu = \frac{2m_1m_2}{(m_1+m_2)}, \\ M_{BG} = 2.24\sqrt{A} = 0.95 \text{ GeV}, \\ \Lambda = 414 \text{ MeV}, \\ \eta_f = \begin{cases} 4, & Q = Q' = c, \\ 5, & Q, Q' = c, b, \end{cases} \end{cases} \tag{11}$$

where the scale μ is chosen to be equal to the reduced constituents mass, M_{BG} is the background mass, Λ is the parameter of the running coupling constant obtained from the analysis of meson mass spectra and η_f is the number of open flavors. $D_{\mu\nu}(\mathbf{k})$ is the gluon propagator in the Coulomb gauge:

$$\begin{cases} D^{00}(\mathbf{k}) = -\frac{4\pi}{\mathbf{k}^2}, \\ D^{ij}(\mathbf{k}) = -\frac{4\pi}{k^2}\left(\delta^{ij} - \frac{k^i k^j}{\mathbf{k}^2}\right), \qquad i,j = \overline{1,3}. \\ D^{0i} = D^{i0} = 0, \end{cases} \tag{12}$$

Γ^{μ}_{l} is the effective long-range vector interaction vertex [25]. It contains both Dirac and Pauli terms:

$$\Gamma_{l;\mu}(\mathbf{k}) = \gamma_\mu + \frac{i\kappa}{2m_l}\sigma_{\mu\nu}\tilde{k}^\nu, \quad \tilde{k} = (0,\mathbf{k}), \quad l = 1,2, \tag{13}$$

where $\sigma_{\mu\nu}$ is the commutator of the Dirac matrices, κ is the long-range anomalous chromomagnetic moment of quarks, and $\frac{i\kappa}{2m_l}\sigma_{\mu\nu}\tilde{k}^\nu$ is the anomalous chromomagnetic interaction. $V^{\text{v, s}}_{\text{conf.}}$ are the vector and scalar confining potentials, which in the nonrelativistic limit in configuration space (consistent with the lattice calculations) have the form

$$\begin{gathered} V^{V}_{\text{conf.}}(r) = (1-\varepsilon)V_{\text{conf.}}(r), \\ V^{S}_{\text{conf.}}(r) = \varepsilon V_{\text{conf.}}(r), \\ V^{V}_{\text{conf.}}(r) + V^{S}_{\text{conf.}}(r) = V_{\text{conf.}}(r) = Ar + B, \end{gathered} \tag{14}$$

where ε is the mixing coefficient. Therefore, in the nonrelativistic limit, the QQ' quasipotential reduces to

$$V^{\text{NR}}_{QQ'}(r) = \frac{1}{2}V^{\text{NR}}_{Q\bar{Q}'}(r) = \frac{1}{2}\Big(-\frac{4}{3}\frac{\alpha_s}{r} + Ar + B\Big), \tag{15}$$

reproducing the usual Cornell potential. Thus, our quasipotential can be viewed as its relativistic generalization. It contains both spin-independent and spin-dependent relativistic contributions.

Constructing the diquark–antidiquark quasipotential, we use the same assumptions about the structure of the short- and long-range interactions. We also take into account the finite size of the diquarks and their integer spin. The quasipotential then is given by [22,26]

$$V(\mathbf{p},\mathbf{q};M) = \underbrace{\frac{<d(\mathcal{P})|J_\mu|d(\mathcal{Q})>}{2\sqrt{E_d}\sqrt{E_d}}\frac{4}{3}\alpha_s D^{\mu\nu}(\mathbf{k})\frac{<d'(\mathcal{P}')|J_\nu|d'(\mathcal{Q}')>}{2\sqrt{E_{d'}}\sqrt{E_{d'}}}}_{\text{diquark}-\text{gluon interation}}$$

$$+ \underbrace{\Psi^*_d(\mathcal{P})\Psi^*_{d'}(\mathcal{P}')[J_{d;\mu}J^{\mu}_{d'}V^{V}_{\text{conf.}}(\mathbf{k}) + V^{S}_{\text{conf.}}(\mathbf{k})]\Psi_d(\mathcal{Q})\Psi_{d'}(\mathcal{Q}')}_{\text{confinement}}. \tag{16}$$

Here, d and d' denote the diquark and antidiquark, $\mathcal{Q}^{(')} = (E_{d^{(')}} \pm \mathbf{q})$ and $\mathcal{P}^{(')} = (E_{d^{(')}}, \pm\mathbf{p})$ are the initial and final diquark momenta, respectively, $k = \mathcal{P} - \mathcal{Q}$, $E_{d,d'}$ are the on-shell diquark energies (similar to Equation (3)):

$$\begin{cases} E_d = \frac{M^2 - M_{d'}^2 + M_d^2}{2M}, \\ E_{d'} = \frac{M^2 - M_d^2 + M_{d'}^2}{2M}, \end{cases} \tag{17}$$

where $M_{d,d'}$ are the diquark and antidiquark masses. $\Psi_d(p)$ is the diquark wave function:

$$\Psi_d(p) = \begin{cases} 1, & \text{scalar} \\ \epsilon_d(p), & \text{axialvector} \end{cases} \quad \text{diquarks}, \tag{18}$$

where $\epsilon_d(p)$ is the polarization vector of an axialvector diquark with momentum $\mathbf{p}$:

$$\epsilon_d(p) = \left(\frac{(\boldsymbol{\epsilon_d}\mathbf{p})}{M_d}, \boldsymbol{\epsilon_d} + \frac{(\boldsymbol{\epsilon_d}\mathbf{p})\mathbf{p}}{M_d(M_d + E_d(p))} \right), \tag{19}$$

$$\epsilon_d^{\mu}(p) p_{\mu} = 0,$$

where $E_d(p)$ is the diquark energy (similar to Equation (8)):

$$E_d(p) = \sqrt{M_d^2 + \mathbf{p}^2}. \tag{20}$$

$J_{d;\mu}$ is the effective long-range vector interaction vertex of the diquark:

$$J_{d;\mu} = \begin{cases} \frac{(\mathcal{P}+Q)_{\mu}}{2\sqrt{E_d}\sqrt{E_d}}, & \text{scalar} \\ -\frac{(\mathcal{P}+Q)_{\mu}}{2\sqrt{E_d}\sqrt{E_d}} + \frac{i\mu_d}{2M_d} \sum_{\mu}^{\nu} \tilde{k}_{\nu}, & \text{axialvector} \end{cases} \quad \text{diquarks}, \tag{21}$$

$$\mu_d = 0, \tag{22}$$

where μ_d is the total chromomagnetic moment of the diquark, which we choose to be equal to zero to vanish the long-range chromomagnetic interaction. $(\sum_{\rho\sigma})_{\mu}^{\nu}$ is a fully antisymmetric tensor:

$$(\sum_{\rho\sigma})_{\mu}^{\nu} = -i(g_{\mu\rho}\delta_{\sigma}^{\nu} - g_{\mu\sigma}\delta_{\rho}^{\nu}). \tag{23}$$

$< d(\mathcal{P})|J_{\mu}|d(\mathcal{Q}) >$ is the diquark–gluon interaction vertex (Figure 1), which accounts for the internal structure of the diquark and leads to the emergence of the form factor $F(r)$ smearing the one-gluon exchange potential [21]:

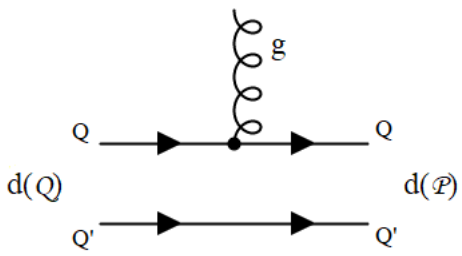

Figure 1. Feynman diagram of the gluon emission by a quark in a diquark.

$$< d(\mathcal{P})|J_{\mu}|d(\mathcal{Q}) >= \int \frac{d^3p\, d^3q}{(2\pi)^6} \, \overline{\Psi}_d^{\mathcal{P}}(\mathbf{p}) \Gamma_{\mu}(\mathbf{p},\mathbf{q}) \Psi_d^{\mathcal{Q}}(\mathbf{q}). \tag{24}$$

Here J_μ is the quark current:

$$J_\mu = \bar{Q}\gamma_\mu Q, \tag{25}$$

where $Q, \bar{Q}$ denote the initial and final states of the quark, respectively. $\Gamma_\mu(\mathbf{p}, \mathbf{q})$ is the vertex function of the diquark interaction with the gluon field [27,28]:

$$\Gamma^\mu(\mathbf{p}, \mathbf{q}) = \overline{u}_{Q_1}(p_1)\gamma^\mu u_{Q_1}(q_1)(2\pi)^3\delta(\mathbf{p_2} - \mathbf{q_2}) + \overline{u}_{Q_2}(p_2)\gamma^\mu u_{Q_2}(q_2)(2\pi)^3\delta(\mathbf{p_1} - \mathbf{q_1}), \tag{26}$$

$$\begin{cases} q_l = \varepsilon_l(q)\frac{\mathcal{Q}}{M_d(q)} \pm \sum\limits_{i=1}^{3} n^{(i)}(\mathcal{Q})q^i, \\ p_l = \varepsilon_l(p)\frac{\mathcal{P}}{M_d(p)} \pm \sum\limits_{i=1}^{3} n^{(i)}(\mathcal{P})p^i, \\ n^{(i)\mu}(\mathcal{Q}) = \left\{ \frac{\mathcal{Q}^i}{M_d}, \ \delta_{ij} + \frac{\mathcal{Q}^i\mathcal{Q}^j}{M_d(q)(E_d(\mathcal{Q}) + M_d(q))} \right\}, \\ M_d(q) = \varepsilon_1(q) + \varepsilon_2(q), \end{cases} \qquad l = 1, 2 \equiv Q, Q'. \tag{27}$$

To take into account the finite size of the diquark, it is necessary to calculate the matrix elements of quark currents between diquarks $< d(\mathcal{P})|J_\mu|d(\mathcal{Q}) >$. These matrix elements are elastic (diagonal) and can be parametrized by the set of form factors $h_{+,1,2,3}(k^2)$ [21]. For a scalar diquark,

$$< S(\mathcal{P})|J_\mu|S(\mathcal{Q}) >= h_+(k^2)(\mathcal{P} + \mathcal{Q})_\mu, \tag{28}$$

For an axialvector diquark,

$$\begin{aligned} < A(\mathcal{P})|J_\mu|A(\mathcal{Q}) > = & -h_1(k^2)\Big[\epsilon_d^*(\mathcal{P}) \cdot \epsilon_d(\mathcal{Q})\Big](\mathcal{P} + \mathcal{Q})_\mu \\ & + h_2(k^2)\Big\{\Big[\epsilon_d^*(\mathcal{P}) \cdot \mathcal{Q}\Big]\epsilon_{d;\mu}(\mathcal{Q}) + \Big[\epsilon_d(\mathcal{Q}) \cdot \mathcal{P}\Big]\epsilon_{d;\mu}^*(\mathcal{P})\Big\} \\ & + h_3(k^2)\frac{1}{M_A^2}\Big[\epsilon_d^*(\mathcal{P}) \cdot \mathcal{Q}\Big]\Big[\epsilon_d(\mathcal{Q}) \cdot \mathcal{P}\Big](\mathcal{P} + \mathcal{Q})_\mu, \end{aligned} \tag{29}$$

where M_A is the mass of the axialvector diquark.

The calculation shows that [16]

$$\begin{cases} h_+(k^2) = h_1(k^2) = h_2(k^2) = F(\mathbf{k}^2), \\ h_3(k^2) = 0, \end{cases} \tag{30}$$

where $F(\mathbf{k}^2)$ is the form factor in the momentum space:

$$\begin{aligned} F(\mathbf{k}^2) = & \frac{\sqrt{M_d E_d}}{M_d + E_d}\int\frac{d^3p}{(2\pi)^3}\Bigg\{\Bigg[\overline{\Psi}_d\Big(\mathbf{p} + \frac{2\varepsilon_{Q_2}(p)}{M_d + E_d}\mathbf{k}\Big)\sqrt{\frac{\varepsilon_{Q_1}(p) + m_{Q_1}}{\varepsilon_{Q_1}(p+k) + m_{Q_1}}} \\ & \times\Big(\frac{\varepsilon_{Q_1}(p+k) + \varepsilon_{Q_1}(p)}{2\sqrt{\varepsilon_{Q_1}(p+k)\varepsilon_{Q_1}(p)}} + \frac{\mathbf{pk}}{2(\varepsilon_{Q_1}(p) + m_{Q_1})\sqrt{\varepsilon_{Q_1}(p+k)\varepsilon_{Q_1}(p)}}\Big)\Psi_d(\mathbf{p})\Bigg] \\ & + \Bigg[\overline{\Psi}_d\Big(\mathbf{p} + \frac{2\varepsilon_{Q_1}(p)}{M_d + E_d}\mathbf{k}\Big)\sqrt{\frac{\varepsilon_{Q_2}(p) + m_{Q_2}}{\varepsilon_{Q_2}(p+k) + m_{Q_2}}} \\ & \times\Big(\frac{\varepsilon_{Q_2}(p+k) + \varepsilon_{Q_2}(p)}{2\sqrt{\varepsilon_{Q_2}(p+k)\varepsilon_{Q_2}(p)}} + \frac{\mathbf{pk}}{2(\varepsilon_{Q_2}(p) + m_{Q_2})\sqrt{\varepsilon_{Q_2}(p+k)\varepsilon_{Q_2}(p)}}\Big)\Psi_d(\mathbf{p})\Bigg]\Bigg\}. \end{aligned} \tag{31}$$

The form factor $F(r)$ is determined by the Fourier transform of the $\frac{F(\mathbf{k}^2)}{\mathbf{k}^2}$ which is then multiplied by r. Numerical calculations show that it can be parameterized with high accuracy as [21]

$$F(r) = 1 - e^{-\xi r - \zeta r^2}. \tag{32}$$

These form factors are shown in Figure 2.

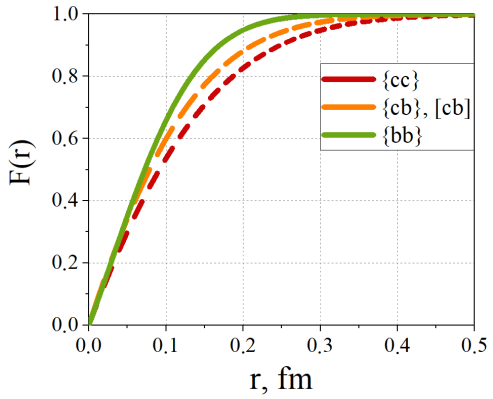

Figure 2. Form factors $F(r)$ for the various doubly heavy diquarks. $\{Q, Q'\}$ denotes axialvector and $[Q, Q']$ denotes scalar diquarks, respectively.

Finally, we obtain the diquark–antidiquark interaction potential [15,26]:

$$V(r) = \Bigg[V_{\text{Coul.}}(r) + V_{\text{conf.}}(r) + \frac{1}{E_1 E_2}\Bigg\{\mathbf{p}\Big[V_{\text{Coul.}}(r) + V^V_{\text{conf.}}(r)\Big]\mathbf{p} - \frac{1}{4}\Delta V^V_{\text{conf.}}(r) + V'_{\text{Coul.}}(r)\frac{\mathbf{L}^2}{2r}\Bigg\}\Bigg] \tag{33.1}$$

$$+\Bigg[\Bigg\{\frac{1}{2}\Bigg[\frac{1}{E_1(E_1+M_1)} + \frac{1}{E_2(E_2+M_2)}\Bigg]\frac{V'_{\text{Coul.}}(r)}{r} - \frac{1}{2}\Bigg[\frac{1}{M_1(E_1+M_1)} + \frac{1}{M_2(E_2+M_2)}\Bigg]\frac{V'_{\text{conf.}}(r)}{r} + \frac{\mu_d}{4}\Bigg[\frac{1}{M_1^2} + \frac{1}{M_2^2}\Bigg]\frac{V'^V_{\text{conf.}}(r)}{r} + \frac{1}{E_1 E_2}\Bigg[V'_{\text{Coul.}}(r) + \frac{\mu_d}{4}\Big(\frac{E_1}{M_1} + \frac{E_2}{M_2}\Big)V'^V_{\text{conf.}}(r)\Bigg]\frac{1}{r}\Bigg\}\mathbf{L}(\mathbf{S_1}+\mathbf{S_2}) + \Bigg\{\frac{1}{2}\Bigg[\frac{1}{E_1(E_1+M_1)} - \frac{1}{E_2(E_2+M_2)}\Bigg]\frac{V'_{\text{Coul.}}(r)}{r} - \frac{1}{2}\Bigg[\frac{1}{M_1(E_1+M_1)} - \frac{1}{M_2(E_2+M_2)}\Bigg]\frac{V'_{\text{conf.}}(r)}{r} + \frac{\mu_d}{4}\Bigg[\frac{1}{M_1^2} - \frac{1}{M_2^2}\Bigg]\frac{V'^V_{\text{conf.}}(r)}{r} + \frac{1}{E_1 E_2}\frac{\mu_d}{4}\Big(\frac{E_1}{M_1} - \frac{E_2}{M_2}\Big)\frac{V'^V_{\text{conf.}}(r)}{r}\Bigg\}\mathbf{L}(\mathbf{S_1}-\mathbf{S_2})\Bigg] \tag{33.2}$$

$$+\Bigg[\frac{1}{3E_1E_2}\Bigg\{\frac{1}{r}V'_{\text{Coul.}}(r) - V''_{\text{Coul.}}(r) + \frac{\mu_d^2}{4}\frac{E_1E_2}{M_1M_2}\Big(\frac{1}{r}V'^V_{\text{conf.}}(r) - V''^V_{\text{conf.}}(r)\Big)\Bigg\} \times \Bigg[\frac{3}{r^2}\Big(\mathbf{S_1 r}\Big)\Big(\mathbf{S_2 r}\Big) - \mathbf{S_1 S_2}\Bigg]\Bigg] \tag{33.3}$$

$$+\Bigg[\frac{2}{3E_1E_2}\Bigg\{\Delta V_{\text{Coul.}}(r) + \frac{\mu_d^2}{4}\frac{E_1E_2}{M_1M_2}\Delta V^V_{\text{conf.}}(r)\Bigg\}\mathbf{S_1 S_2}\Bigg], \tag{33.4}$$

where $\mathbf{p}$ is the relative momentum, $M_{1,2}$ and $E_{1,2}$ are the masses and energies of the diquark and antidiquark, μ_d is the total chromomagnetic moment of the diquark (we chose it to be zero), $\mathbf{S_d}$ is the axialvector diquark spin, $\mathbf{L}$ is the relative orbital momentum of the system, and $V_{\text{conf.}}$ is the confining potential in the nonrelativistic limit:

$$V_{\text{conf.}} = V^V_{\text{conf.}} + V^S_{\text{conf.}} = (1-\varepsilon)(Ar+B) + \varepsilon(Ar+B) = Ar + B, \tag{34}$$

where ε are the scalar and vector confinement mixing coefficient, and the Coulomb potential $V_{\text{Coul.}}(r)$ is taken to be

$$V_{\text{Coul.}}(r) \equiv -\frac{4}{3}\alpha_s \frac{F_1(r)F_2(r)}{r}. \tag{35}$$

$F_{1,2}(r)$ are the form factors that take into account the diquark sizes (Equation (32)).

In Equation (33), we explicitly separated the spin-independent (33.1) and spin-dependent terms: (33.2) for the spin–orbit, (33.3) for the tensor and (33.4) for the spin–spin interactions.

First, we calculate the masses and wave functions of the doubly heavy (anti)diquarks as the bound (anti)quark-(anti)quark states. It is done by solving Equation (1) with the quasipotential (5), (6)–(14) numerically. Then the masses of the tetraquarks and their wave functions are obtained for the bound diquark–antidiquark states with the same method.

Parameters such as the confinement potential mixing coefficient ε, anomalous chromomagnetic moment κ, parameter of the running coupling constant Λ, confining potential parameters A, B and quark masses $m_{c,b}$ are taken from our previous works on the study of the properties of mesons and baryons [25,29–31] and are given in the Table 1. The diquark masses $M_{cc,cb,bb}$ and the parameters of their form factors ξ and ζ were already calculated earlier [21,26] and are given in Table 2.

Table 1. Parameters of the model [25,29–31].

m_c, GeV	m_b, GeV	A, GeV^2	B, GeV	Λ, MeV	ε	κ
1.55	4.88	0.18	−0.3	414	−1	−1

Table 2. Masses $M_{QQ'}$ and form factor parameters ξ, ζ of diquarks. d is the axialvector (A) or scalar (S) diquark. $[Q,Q']$ and $\{Q,Q'\}$ denote combinations of quarks antisymmetric and symmetric in flavor, respectively [21,26].

QQ'	$\mathbf{d}$	$Q=c$			$Q=b$		
		M_{cQ}, MeV	ξ, GeV	ζ, GeV^2	M_{bQ}, MeV	ξ, GeV	ζ, GeV^2
$[Q,c]$	S				6519	1.50	0.59
$\{Q,c\}$	A	3226	1.30	0.42	6526	1.50	0.59
$\{Q,b\}$	A	6526	1.50	0.59	9778	1.30	1.60

4. Masses of Fully Heavy Tetraquarks

The calculated mass spectra of fully heavy tetraquarks are given in Table 3. Masses of the ground states (1S) of all possible nine compositions of fully heavy tetraquarks (including symmetrical: $cc\bar{c}\bar{c}$, $cb\bar{c}\bar{b}$, $bb\bar{b}\bar{b}$, "mirrored": $cc\bar{b}\bar{b}$, $bb\bar{c}\bar{c}$ and nonsymmetrical: $cc\bar{c}\bar{b}, cb\bar{c}\bar{c}$, $cb\bar{b}\bar{b}$, $bb\bar{c}\bar{b}$) have already been calculated in our previous work (we corrected the small numerical error in our original calculation of the ground $cb\bar{c}\bar{b}$ states.) [14].

As it already was discussed in Section 2, a scalar (anti)diquark can be a part of a tetraquark only if the (anti)quarks that form it have different flavors. This means that the $cc\bar{c}\bar{c}$ and $bb\bar{b}\bar{b}$ tetraquarks can consist only of axialvector diquarks and antidiquarks, while $cb\bar{c}\bar{b}$ can also consist of a scalar and a mixture of axialvector and scalar diquarks and antidiquarks. As the result, we obtain more possible states for $cb\bar{c}\bar{b}$: an additional 12 mixed and 6 scalar states are added to 32 axialvector states.

As we see from Table 3, the diquark–antidiquark model of the tetraquarks predicts too many states, but not all of them can be observed experimentally due to the fast decay into two heavy mesons through the quark rearrangement. To limit the number of predicted states, we consider diquarks only in the ground color triplet state and assume that all excitations occur between the diquark and antidiquark. These excited states have more chances to be observed as resonances since such excitations lead to a larger separation between the diquark and antidiquark, increasing the mean distance between the heavy quark and antiquark, and thus reducing the probability of the fall-apart decay process. Contrarily, excitations within the diquark or/and antidiquark increase the diquark mass and thus produce a larger overlap between the diquark and antidiquark, which enhances the fall-apart decay processes. The chances that the predicted tetraquark states will be observed experimentally as relatively narrow resonances increase if their decays are suppressed by the phase space, which is determined by the difference between the tetraquark mass and the meson pair decay threshold. This issue is discussed in detail in the following section. However, the width of the resonance does not only depend on the phase space in the decay channel [32]. The excited states of the tetraquarks can be narrow, despite the large phase space, since it is necessary to overcome the suppression in the fall-apart process, either due to the centrifugal barrier for the orbital excitations or due to the presence of the nodes in the wave function of the radially excited state. This result is well-known from the study of exotic atoms where some of the states with a higher mass have smaller widths notwithstanding the larger phase space for the decay [33]. This occurs when the annihilation potential is added. Then the wave function is further pushed out of the conversion region reducing the overlap between the coupling potential and the square of the wave function, thus decreasing the decay width. The quantitative analysis of such decays is beyond the scope of the present paper. Note that in the literature, the arguments that some of these tetraquarks should be unbound were given on the basis of the hyperspherical harmonic expansion [34], the string dynamics [35], and the Hall–Post inequalities [36].

5. Threshold Analysis

If a mass of the tetraquark exceeds the sum of the masses of a meson pair composed of the same flavor quarks and antiquarks and its decay is not forbidden by quantum numbers (spin-parity J^{PC}), then the tetraquark will decay into this meson pair through the quark rearrangement via the strong interaction. This is the so-called fall-apart process, whose rate is governed by the difference of the tetraquark and threshold masses. If a mass of the tetraquark lies below the corresponding threshold, the decay is possible due to the heavy quark–antiquark annihilation into gluons or a radiative decay, but such processes are suppressed, making these tetraquarks narrow states.

In Tables 4–8, comparisons of the mass spectra of fully heavy tetraquarks, calculated by us (Table 3), with the meson pair decay thresholds are given. The values of the phase volume Δ are of special interest:

$$\Delta = M_{QQ'\bar{Q}\bar{Q}'} - M_{thr}, \tag{36}$$

where $M_{QQ'\bar{Q}\bar{Q}'}$ is the tetraquark mass and M_{thr} is the meson pair decay threshold. We are interested in the most probable decay modes for each tetraquark. They, in turn, correspond to the largest of possible values of Δ: Δ_{max}. Therefore, in Tables 4–8, we compare tetraquark masses not with all possible thresholds, but only with the lowest ones ($[M_{\rm thr}]_{\rm min} \to \Delta_{\rm max} \to$ more probable decay mode).

Table 3. Masses $M_{QQ'\bar{Q}\bar{Q}'}$ of the ground (1S) and excited (1P, 2S, 1D, 2P, 3S) $cc\bar{c}\bar{c}$, $cb\bar{c}\bar{b}$, $bb\bar{b}\bar{b}$ states. d and $\bar{d}'$ are the axialvector (A) or scalar (S) diquark and antidiquark, respectively. S is the total spin of the diquark–antidiquark system. All masses are given in MeV.

$d\bar{d}'$	State	S	J^{PC}	$M_{cc\bar{c}\bar{c}}$	$M_{cb\bar{c}\bar{b}}$	$M_{bb\bar{b}\bar{b}}$
$A\bar{A}$	1S	0	0^{++}	6190	12,838	19,314
		1	1^{+-}	6271	12,855	19,320
		2	2^{++}	6367	12,883	19,330
	1P	0	1^{--}	6631	13,103	19,536
		1	0^{-+}	6628	13,100	19,533
			1^{-+}	6634	13,103	19,535
			2^{-+}	6644	13,108	19,539
		2	1^{--}	6635	13,103	19,534
			2^{--}	6648	13,109	19,538
			3^{--}	6664	13,116	19,545
	2S	0	0^{++}	6782	13,247	19,680
		1	1^{+-}	6816	13,256	19,682
		2	2^{++}	6868	13,272	19,687
	1D	0	2^{++}	6921	13,306	19,715
		1	1^{+-}	6909	13,299	19,710
			2^{+-}	6920	13,304	19,714
			3^{+-}	6932	13,311	19,720
		2	0^{++}	6899	13,293	19,705
			1^{++}	6904	13,296	19,707
			2^{++}	6915	13,301	19,711
			3^{++}	6929	13,308	19,717
			4^{++}	6945	13,317	19,724
	2P	0	1^{--}	7091	13,428	19,820
		1	0^{-+}	7100	13,431	19,821
			1^{-+}	7099	13,431	19,821
			2^{-+}	7098	13,431	19,822
		2	1^{--}	7113	13,434	19,823
			2^{--}	7113	13,435	19,823
			3^{--}	7112	13,436	19,824
	3S	0	0^{++}	7259	13,558	19,941
		1	1^{+-}	7287	13,566	19,943
		2	2^{++}	7333	13,580	19,947
$\frac{1}{\sqrt{2}}\left(A\bar{S} \pm S\bar{A}\right)$	1S	1	$1^{+\pm}$		12,863	
	1P		$0^{-\pm}$		13,096	
			$1^{-\pm}$		13,099	
			$2^{-\pm}$		13,104	
	2S		$1^{+\pm}$		13,257	
	1D		$1^{+\pm}$		13,293	
			$2^{+\pm}$		13,298	
			$3^{+\pm}$		13,305	
	2P		$0^{-\pm}$		13,426	
			$1^{-\pm}$		13,426	
			$2^{-\pm}$		13,427	
	3S		$1^{+\pm}$		13,566	
$S\bar{S}$	1S	0	0^{++}		12,856	
	1P		1^{--}		13,095	
	2S		0^{++}		13,250	
	1D		2^{++}		13,293	
	2P		1^{--}		13,420	
	3S		0^{++}		13,559	

Table 4. Masses M of the ground (1S) and excited (1P, 2S, 1D, 2P, 3S) $cc\bar{c}\bar{c}$ states composed from the axialvector diquarks (Table 3) and the corresponding meson–meson thresholds. d and $\bar{d}'$ are the axialvector (A) or scalar (S) diquark and antidiquark, respectively. S is the total spin of the diquark–antidiquark system. M_{thr} is the corresponding meson–meson threshold [2]. Δ is the difference between the tetraquark mass and threshold: $\Delta = M - M_{thr}$. All masses are given in MeV. For the states with the maximum Δ (corresponding to lightest threshold, main decay channel) less than 300 MeV, all possible thresholds and their Δ are given. For the states with maximum Δ above 300 MeV, only the lightest thresholds are shown. The states with maximum Δ less than 100 MeV are additionally highlighted in violet as most promising to be stable. We also give thresholds with a small negative Δ, since we do not take into account the errors of theoretical calculations. The candidates for the states recently observed by LHCb [5], CMS [6] and ATLAS [7] are highlighted in color: turquoise for X(6200) (ATLAS), emerald for X(6400) (LHCb) and X(6600) (CMS, ATLAS), green for X(6900) (LHCb, CMS, ATLAS), blue for X(7200) (LHCb, ATLAS) and X(7300) (CMS). Additionally, all di-J/ψ thresholds are shown in bold since these meson pairs are easiest to study in experiments.

$QQ\bar{Q}\bar{Q}$	$d\bar{d}'$	State	S	J^{PC}	M	M_{thr}	Δ	Meson Pair
$cc\bar{c}\bar{c}$	$A\bar{A}$	1S	0	0^{++}	**6190**	5968	222	$\eta_c(1S)\eta_c(1S)$
						6194	−4	$\boldsymbol{J/\psi(1S)J/\psi(1S)}$
			1	1^{+-}	6271	6081	190	$\eta_c(1S)J/\psi(1S)$
			2	2^{++}	**6367**	**6194**	**173**	$\boldsymbol{J/\psi(1S)J/\psi(1S)}$
		1P	0	1^{--}	6631	6509	122	$\eta_c(1S)h_c(1P)$
						6512	119	$J/\psi(1S)\chi_{c0}(1P)$
						6608	23	$J/\psi(1S)\chi_{c1}(1P)$
			1	0^{-+}	6628	6399	229	$\eta_c(1S)\chi_{c0}(1P)$
						6622	6	$J/\psi(1S)h_c(1P)$
				1^{-+}	6634	6495	139	$\eta_c(1S)\chi_{c1}(1P)$
						6622	12	$J/\psi(1S)h_c(1P)$
				2^{-+}	6644	6540	104	$\eta_c(1S)\chi_{c2}(1P)$
						6622	22	$J/\psi(1S)h_c(1P)$
			2	1^{--}	6635	6509	126	$\eta_c(1S)h_c(1P)$
						6512	123	$J/\psi(1S)\chi_{c0}(1P)$
						6608	27	$J/\psi(1S)\chi_{c1}(1P)$
						6653	−18	$J/\psi(1S)\chi_{c2}(1P)$
				2^{--}	6648	6608	40	$J/\psi(1S)\chi_{c1}(1P)$
						6653	−5	$J/\psi(1S)\chi_{c2}(1P)$
				3^{--}	6664	6653	11	$J/\psi(1S)\chi_{c2}(1P)$
		2S	0	0^{++}	**6782**[1]	5968	814	$\eta_c(1S)\eta_c(1S)$
						6194	**588**	$\boldsymbol{J/\psi(1S)J/\psi(1S)}$
			1	1^{+-}	6816	6081	735	$\eta_c(1S)J/\psi(1S)$
			2	2^{++}	**6868**	**6194**	**674**	$\boldsymbol{J/\psi(1S)J/\psi(1S)}$
		1D	0	2^{++}	**6921**	**6194**	**727**	$\boldsymbol{J/\psi(1S)J/\psi(1S)}$
			1	1^{+-}	6909	6081	828	$\eta_c(1S)J/\psi(1S)$
				2^{+-}	6920	6808	112	$\eta_c(1S)\psi_2(3823)$
				3^{+-}	6932	6827	105	$\eta_c(1S)\psi_3(3842)$
			2	0^{++}	**6899**	5968	931	$\eta_c(1S)\eta_c(1S)$
						6194	**705**	$\boldsymbol{J/\psi(1S)J/\psi(1S)}$
				1^{++}	**6904**	**6194**	**710**	$\boldsymbol{J/\psi(1S)J/\psi(1S)}$
				2^{++}	**6915**	**6194**	**721**	$\boldsymbol{J/\psi(1S)J/\psi(1S)}$
				3^{++}	6929	6921	8	$J/\psi(1S)\psi_2(3823)$
						6940	19	$J/\psi(1S)\psi_3(3842)$
				4^{++}	6945	6940	5	$J/\psi(1S)\psi_3(3842)$

Table 4. *Cont.*

$QQ\bar{Q}\bar{Q}$	$d\bar{d}'$	State	S	J^{PC}	M	M_{thr}	Δ	Meson Pair
$cc\bar{c}\bar{c}$	$A\bar{A}$	2P	0	1^{--}	7091	6509	582	$\eta_c(1S)h_c(1P)$
			1	0^{-+}	7100	6399	701	$\eta_c(1S)\chi_{c0}(1P)$
				1^{-+}	7099	6495	604	$\eta_c(1S)\chi_{c1}(1P)$
				2^{-+}	7098	6540	558	$\eta_c(1S)\chi_{c2}(1P)$
			2	1^{--}	7113	6509	604	$\eta_c(1S)h_c(1P)$
				2^{--}	7113	6608	505	$J/\psi(1S)\chi_{c1}(1P)$
				3^{--}	7112	6653	459	$J/\psi(1S)\chi_{c2}(1P)$
		3S	0	0^{++}	**7259**	5968	1291	$\eta_c(1S)\eta_c(1S)$
						6194	**1065**	$\boldsymbol{J/\psi(1S)J/\psi(1S)}$
			1	1^{+-}	7287	6081	1206	$\eta_c(1S)J/\psi(1S)$
			2	2^{++}	**7333**[2]	**6194**	**1139**	$\boldsymbol{J/\psi(1S)J/\psi(1S)}$

[1] Candidate only for the X(6600) state. [2] Candidate only for the X(7300) state.

Table 5. Same as in Table 4 but for $cb\bar{c}\bar{b}$ states composed from the axialvector (A) diquarks. Colors are explained in the caption of Table 4.

$QQ\bar{Q}\bar{Q}$	$d\bar{d}'$	State	S	J^{PC}	M	M_{thr}	Δ	Meson Pair
$cb\bar{c}\bar{b}$	$A\bar{A}$	1S	0	0^{++}	12,838	12,383	455	$\eta_c(1S)\eta_b(1S)$
			1	1^{+-}	12,855	12,444	411	$\eta_c(1S)\Upsilon(1S)$
			2	2^{++}	12,883	12,557	326	$J/\psi(1S)\Upsilon(1S)$
		1P	0	1^{--}	13,103	12,875	228	$\chi_{c0}(1P)\Upsilon(1S)$
						12,883	220	$\eta_c(1S)h_b(1P)$
						12,924	179	$h_c(1P)\eta_b(1S)$
						12,956	147	$J/\psi(1S)\chi_{b0}(1P)$
						12,971	132	$\chi_{c1}(1P)\Upsilon(1S)$
						12,990	113	$J/\psi(1S)\chi_{b1}(1P)$
						13,009	94	$J/\psi(1S)\chi_{b2}(1P)$
						13,016	87	$\chi_{c2}(1P)\Upsilon(1S)$
			1	0^{-+}	13,100	12,813	287	$\chi_{c0}(1P)\eta_b(1S)$
						12,843	257	$\eta_c(1S)\chi_{b0}(1P)$
						12,986	114	$h_c(1P)\Upsilon(1S)$
						12,996	104	$J/\psi(1S)h_b(1P)$
				1^{-+}	13,103	12,877	226	$\eta_c(1S)\chi_{b1}(1P)$
						12,909	194	$\chi_{c1}(1P)\eta_b(1S)$
						12,986	117	$h_c(1P)\Upsilon(1S)$
						12,996	107	$J/\psi(1S)h_b(1P)$
				2^{-+}	13,108	12,896	212	$\eta_c(1S)\chi_{b2}(1P)$
						12,955	153	$\chi_{c2}(1P)\eta_b(1S)$
						12,986	122	$h_c(1P)\Upsilon(1S)$
						12,996	112	$J/\psi(1S)h_b(1P)$
			2	1^{--}	13,103	12,875	228	$\chi_{c0}(1P)\Upsilon(1S)$
						12,883	220	$\eta_c(1S)h_b(1P)$
						12,924	179	$h_c(1P)\eta_b(1S)$
						12,956	147	$J/\psi(1S)\chi_{b0}(1P)$
						12,971	132	$\chi_{c1}(1P)\Upsilon(1S)$
						12,990	113	$J/\psi(1S)\chi_{b1}(1P)$
						13,009	94	$J/\psi(1S)\chi_{b2}(1P)$
						13,016	87	$\chi_{c2}(1P)\Upsilon(1S)$
				2^{--}	13,109	12,971	138	$\chi_{c1}(1P)\Upsilon(1S)$
						12,990	119	$J/\psi(1S)\chi_{b1}(1P)$
						13,009	100	$J/\psi(1S)\chi_{b2}(1P)$
						13,016	93	$\chi_{c2}(1P)\Upsilon(1S)$
				3^{--}	13,116	13,009	107	$J/\psi(1S)\chi_{b2}(1P)$
						13,016	100	$\chi_{c2}(1P)\Upsilon(1S)$

Table 5. *Cont.*

$QQ\bar{Q}\bar{Q}$	$d\bar{d}'$	State	S	J^{PC}	M	M_{thr}	Δ	Meson Pair
$cb\bar{c}\bar{b}$	$A\bar{A}$	2S	0	0^{++}	13,247	12,383	864	$\eta_c(1S)\eta_b(1S)$
			1	1^{+-}	13,256	12,444	812	$\eta_c(1S)\Upsilon(1S)$
			2	2^{++}	13,272	12,557	715	$J/\psi(1S)\Upsilon(1S)$
		1D	0	2^{++}	13,306	12,557	749	$J/\psi(1S)\Upsilon(1S)$
			1	1^{+-}	13,299	12,444	855	$\eta_c(1S)\Upsilon(1S)$
				2^{+-}	13,304	13,148	156	$\eta_c(1S)\Upsilon_2(1D)$
						13,222	82	$\psi_2(3823)\eta_b(1S)$
				3^{+-}	13,311	13,241	70	$\psi_3(3842)\eta_b(1S)$
			2	0^{++}	13,293	12,383	910	$\eta_c(1S)\eta_b(1S)$
				1^{++}	13,296	12,557	739	$J/\psi(1S)\Upsilon(1S)$
				2^{++}	13,301	12,557	744	$J/\psi(1S)\Upsilon(1S)$
				3^{++}	13,308	13,261	47	$J/\psi(1S)\Upsilon_2(1D)$
						13,284	24	$\psi_2(3823)\Upsilon(1S)$
						13,303	5	$\psi_3(3842)\Upsilon(1S)$
				4^{++}	13,317	13,303	14	$\psi_3(3842)\Upsilon(1S)$
		2P	0	1^{--}	13,428	12,875	553	$\chi_{c0}(1P)\Upsilon(1S)$
			1	0^{-+}	13,431	12,813	618	$\chi_{c0}(1P)\eta_b(1S)$
				1^{-+}	13,431	12,877	554	$\eta_c(1S)\chi_{b1}(1P)$
				2^{-+}	13,431	12,896	535	$\eta_c(1S)\chi_{b2}(1P)$
			2	1^{--}	13,434	12,875	559	$\chi_{c0}(1P)\Upsilon(1S)$
				2^{--}	13,435	12,971	464	$\chi_{c1}(1P)\Upsilon(1S)$
				3^{--}	13,436	13,009	427	$J/\psi(1S)\chi_{b2}(1P)$
		3S	0	0^{++}	13,558	12,383	1175	$\eta_c(1S)\eta_b(1S)$
			1	1^{+-}	13,566	12,444	1122	$\eta_c(1S)\Upsilon(1S)$
			2	2^{++}	13,580	12,557	1023	$J/\psi(1S)\Upsilon(1S)$

From Tables 4–8, a number of conclusions can be drawn. First of all, with the exception of the two following states,

$$X_{bbbb} \quad 1D \quad S=1 \quad 3^{+-} \quad 19,720\ MeV \tag{37}$$

$$X_{bbbb} \quad 1D \quad S=2 \quad 4^{++} \quad 19,724\ MeV, \tag{38}$$

for all other tetraquark states, there is at least one meson pair with a total mass less than the tetraquark mass ($\Delta_{\max} > 0$). Therefore, for almost all tetraquarks, there is a possibility of such fall-apart decay.

For most tetraquarks, the value of Δ_{max} significantly exceeds 300 MeV. These tetraquarks lie significantly higher than the decay thresholds and, thus, they rapidly fall apart in the meson pair due to the quark and antiquark rearrangements. This means that, experimentally, such a state will manifest itself not as a narrow, but as a wide resonance, which is hard to observe. However, such arguments can be applied only to the ground states of tetraquarks. For the excited states, there are additional restrictions. In particular, these decays will be suppressed either by the centrifugal barrier between the quark and antiquark (for the orbital excitations), or by the zeros of the wave function (for the radial excitations), or both simultaneously, and therefore, such tetraquark states can be observed as narrow resonances.

Next, there are also states for which $0 < \Delta_{max} < 300$ MeV. Such states are close to the meson pair decay threshold and, thus, these fall-apart decays have a small phase. For such states, we show in Tables 4–8 not only Δ_{max}, but also all close-lying decay channels and their corresponding Δ in the range $-50 \leq \Delta \leq 300$ MeV. Small negative Δ are given because our calculations have a theoretical error. The uncertainties of our calculations come from the quark model and diquark–antiduark approximation. We roughly estimate them from our previous experience to be about 20–50 MeV. However, if the value of $\Delta_{\max}$ is sufficiently negative, the state cannot decay via the strong fall-apart decay processes into two $Q\bar{Q}'$ quarkonia, and the main channels will be either a decay due to the heavy quark–antiquark annihilation into gluons with their subsequent hadronization into the lighter hadrons (strongly suppressed according to the Okubo–Zweig–Iizuka rule), or radiative decays (if allowed). As a result, this state will be a narrow state that can be observed experimentally in other decay channels: either to hadrons made up of lighter quarks and antiquarks, or two quarkonia and a photon.

Table 6. Same as in Table 4 but for the $cb\bar{c}\bar{b}$ states composed from the mixture of axialvector (A) and scalar (S) diquarks. Colors are explained in the caption of Table 4.

$QQ\bar{Q}\bar{Q}$	$d\bar{d}'$	State	S	J^{PC}	M	M_{thr}	Δ	Meson Pair
$cb\bar{c}\bar{b}$	$\frac{1}{\sqrt{2}}\left(A\bar{S}\pm S\bar{A}\right)$	1S	1	1^{++}	12,863	12,557	306	$J/\psi(1S)\Upsilon(1S)$
				1^{+-}		12,444	419	$\eta_c(1S)\Upsilon(1S)$
		1P		0^{-+}	13,096	12,813	283	$\chi_{c0}(1P)\eta_b(1S)$
						12,843	253	$\eta_c(1S)\chi_{b0}(1P)$
						12,986	110	$h_c(1P)\Upsilon(1S)$
						12,996	100	$J/\psi(1S)h_b(1P)$
				0^{--}		12,971	125	$\chi_{c1}(1P)\Upsilon(1S)$
						12,990	106	$J/\psi(1S)\chi_{b1}(1P)$
				1^{-+}	13,099	12,877	222	$\eta_c(1S)\chi_{b1}(1P)$
						12,909	190	$\chi_{c1}(1P)\eta_b(1S)$
						12,986	113	$h_c(1P)\Upsilon(1S)$
						12,996	103	$J/\psi(1S)h_b(1P)$
				1^{--}		12,875	224	$\chi_{c0}(1P)\Upsilon(1S)$
						12,883	216	$\eta_c(1S)h_b(1P)$
						12,924	175	$h_c(1P)\eta_b(1S)$
						12,956	143	$J/\psi(1S)\chi_{b0}(1P)$
						12,971	128	$\chi_{c1}(1P)\Upsilon(1S)$
						12,990	109	$J/\psi(1S)\chi_{b1}(1P)$
						13,009	90	$J/\psi(1S)\chi_{b2}(1P)$
						13,016	83	$\chi_{c2}(1P)\Upsilon(1S)$
				2^{-+}	13,104	12,896	208	$\eta_c(1S)\chi_{b2}(1P)$
						12,955	149	$\chi_{c2}(1P)\eta_b(1S)$
						12,986	118	$h_c(1P)\Upsilon(1S)$
						12,996	108	$J/\psi(1S)h_b(1P)$
				2^{--}		12,971	133	$\chi_{c1}(1P)\Upsilon(1S)$
						12,990	114	$J/\psi(1S)\chi_{b1}(1P)$
						13,009	114	$J/\psi(1S)\chi_{b2}(1P)$
						13,016	114	$\chi_{c2}(1P)\Upsilon(1S)$
		2S		1^{++}	13,257	12,557	700	$J/\psi(1S)\Upsilon(1S)$
				1^{+-}		12,444	813	$\eta_c(1S)\Upsilon(1S)$
		1D		1^{++}	13,293	12,557	736	$J/\psi(1S)\Upsilon(1S)$
				1^{+-}		12,444	849	$\eta_c(1S)\Upsilon(1S)$
				2^{++}	13,298	12,557	741	$J/\psi(1S)\Upsilon(1S)$
				2^{+-}		13,148	150	$\eta_c(1S)\Upsilon_2(1D)$
						13,222	76	$\psi_2(3823)\eta_b(1S)$
				3^{++}	13,305	13,261	44	$J/\psi(1S)\Upsilon_2(1D)$
						13,284	21	$\psi_2(3823)\Upsilon(1S)$
						13,303	2	$\psi_3(3842)\Upsilon(1S)$
				3^{+-}		13,241	64	$\psi_3(3842)\eta_b(1S)$
		2P		0^{-+}	13,426	12,813	613	$\chi_{c0}(1P)\eta_b(1S)$
				0^{--}		12,971	455	$\chi_{c1}(1P)\Upsilon(1S)$
				1^{-+}	13,426	12,877	549	$\eta_c(1S)\chi_{b1}(1P)$
				1^{--}		12,875	551	$\chi_{c0}(1P)\Upsilon(1S)$
				2^{-+}	13,427	12896	531	$\eta_c(1S)\chi_{b2}(1P)$
				2^{--}		12,971	456	$\chi_{c1}(1P)\Upsilon(1S)$
		3S		1^{++}	13,566	12,557	1009	$J/\psi(1S)\Upsilon(1S)$
				1^{+-}		12,444	1122	$\eta_c(1S)\Upsilon(1S)$

Table 7. Same as in Table 4 but for the $cb\bar{c}\bar{b}$ states composed from the scalar (S) diquarks.

$QQ\bar{Q}\bar{Q}$	$d\bar{d}'$	State	S	J^{PC}	M	M_{thr}	Δ	Meson Pair
$cb\bar{c}\bar{b}$	$S\bar{S}$	1S	0	0^{++}	12,856	12,383	473	$\eta_c(1S)\eta_b(1S)$
		1P		1^{--}	13,095	12,875	220	$\chi_{c0}(1P)\Upsilon(1S)$
						12,883	212	$\eta_c(1S)h_b(1P)$
						12,924	171	$h_c(1P)\eta_b(1S)$
						12,956	139	$J/\psi(1S)\chi_{b0}(1P)$
						12,971	124	$\chi_{c1}(1P)\Upsilon(1S)$
						12,990	105	$J/\psi(1S)\chi_{b1}(1P)$
						13,009	86	$J/\psi(1S)\chi_{b2}(1P)$
						13,016	79	$\chi_{c2}(1P)\Upsilon(1S)$
		2S		0^{++}	13,250	12,383	867	$\eta_c(1S)\eta_b(1S)$
		1D		2^{++}	13,293	12,557	736	$J/\psi(1S)\Upsilon(1S)$
		2P		1^{--}	13,420	12,875	545	$\chi_{c0}(1P)\Upsilon(1S)$
		3S		0^{++}	13,559	12,383	1176	$\eta_c(1S)\eta_b(1S)$

Table 8. Same as in Table 4 but for the $bb\bar{b}\bar{b}$ states composed from the axialvector (A) diquarks. The states with maximum Δ less than 100 MeV are additionally highlighted in violet as most promising to be stable. The states with negative maximum Δ are highlighted in red for the same reason. Additionally, di-$\Upsilon(1S)$ thresholds are shown in bold since these meson pairs are easiest to study in experiments.

$QQ\bar{Q}\bar{Q}$	$dd\bar{d}'$	State	S	J^{PC}	M	M_{thr}	Δ	Meson Pair
$bb\bar{b}\bar{b}$	$A\bar{A}$	1S	0	$\mathbf{0^{++}}$	**19,314**	18,798 **18,921**	516 **393**	$\eta_b(1S)\eta_b(1S)$ **$\Upsilon(1S)\Upsilon(1S)$**
			1	1^{+-}	19,320	18,859	461	$\eta_b(1S)\Upsilon(1S)$
			2	$\mathbf{2^{++}}$	**19,330**	**18,921**	**409**	**$\Upsilon(1S)\Upsilon(1S)$**
		1P	0	1^{--}	19,536	19,298 19,320 19,353 19,373	238 216 183 163	$\eta_b(1S)h_b(1P)$ $\Upsilon(1S)\chi_{b0}(1P)$ $\Upsilon(1S)\chi_{b1}(1P)$ $\Upsilon(1S)\chi_{b2}(1P)$
			1	0^{-+}	19,533	19,258 19,360	275 173	$\eta_b(1S)\chi_{b0}(1P)$ $\Upsilon(1S)h_b(1P)$
				1^{-+}	19,535	19,291 19,360	244 175	$\eta_b(1S)\chi_{b1}(1P)$ $\Upsilon(1S)h_b(1P)$
				2^{-+}	19,539	19,311 19,360	228 179	$\eta_b(1S)\chi_{b2}(1P)$ $\Upsilon(1S)h_b(1P)$
			2	1^{--}	19,534	19,298 19,320 19,353 19,373	236 214 181 161	$\eta_b(1S)h_b(1P)$ $\Upsilon(1S)\chi_{b0}(1P)$ $\Upsilon(1S)\chi_{b1}(1P)$ $\Upsilon(1S)\chi_{b2}(1P)$
				2^{--}	19,538	19,353 19,373	185 165	$\Upsilon(1S)\chi_{b1}(1P)$ $\Upsilon(1S)\chi_{b2}(1P)$
				3^{--}	19,545	19,373	172	$\Upsilon(1S)\chi_{b2}(1P)$
		2S	0	$\mathbf{0^{++}}$	**19,680**	18,798 **18,921**	882 **759**	$\eta_b(1S)\eta_b(1S)$ **$\Upsilon(1S)\Upsilon(1S)$**
			1	1^{+-}	19,682	18,859	823	$\eta_b(1S)\Upsilon(1S)$
			2	$\mathbf{2^{++}}$	**19,687**	**18,921**	**766**	**$\Upsilon(1S)\Upsilon(1S)$**
		1D	0	$\mathbf{2^{++}}$	**19,715**	**18,921**	**794**	**$\Upsilon(1S)\Upsilon(1S)$**
			1	1^{+-}	19,710	18,859	851	$\eta_b(1S)\Upsilon(1S)$
				2^{+-}	19,714	19,562	152	$\eta_b(1S)\Upsilon_2(1D)$
				3^{+-}	19,720	19,812	-92	$h_b(1P)\chi_{b2}(1P)$
			2	$\mathbf{0^{++}}$	**19,705**	18,798 **18,921**	907 **784**	$\eta_b(1S)\eta_b(1S)$ **$\Upsilon(1S)\Upsilon(1S)$**
				$\mathbf{1^{++}}$	**19,707**	**18,921**	**786**	**$\Upsilon(1S)\Upsilon(1S)$**
				$\mathbf{2^{++}}$	**19,711**	**18,921**	**790**	**$\Upsilon(1S)\Upsilon(1S)$**
				3^{++}	19,717	19,624	93	$\Upsilon(1S)\Upsilon_2(1D)$
				4^{++}	19,724	19,824	-100	$\chi_{b2}(1P)\chi_{b2}(1P)$
		2P	0	1^{--}	19,820	19,298	522	$\eta_b(1S)h_b(1P)$
			1	0^{-+}	19,821	19,258	563	$\eta_b(1S)\chi_{b0}(1P)$
				1^{-+}	19,821	19,291	530	$\eta_b(1S)\chi_{b1}(1P)$
				2^{-+}	19,822	19,311	511	$\eta_b(1S)\chi_{b2}(1P)$
			2	1^{--}	19,823	19,298	525	$\eta_b(1S)h_b(1P)$
				2^{--}	19,823	19,353	470	$\Upsilon(1S)\chi_{b1}(1P)$
				3^{--}	19,824	19,373	451	$\Upsilon(1S)\chi_{b2}(1P)$
		3S	0	$\mathbf{0^{++}}$	**19,941**	18,798 **18,921**	1143 **1020**	$\eta_b(1S)\eta_b(1S)$ **$\Upsilon(1S)\Upsilon(1S)$**
			1	1^{+-}	19,943	18,859	1084	$\eta_b(1S)\Upsilon(1S)$
			2	$\mathbf{2^{++}}$	**19,947**	**18,921**	**1026**	**$\Upsilon(1S)\Upsilon(1S)$**

All possible di-J/ψ and di-$\Upsilon(1S)$ decay thresholds are also given in Tables 4–8 (and highlighted in bold). Such decay channels are the most convenient for the experimental studies since these mesons have a characteristic decay into a $\mu^+\mu^-$ pair with branching fractions $\sim 5\%$ and, thus, have a clear experimental signature.

So far, the results of experimental searches are fully correlated with our conclusions. In particular, the LHCb, CMS and ATLAS Collaborations are searching for the fully charmed $cc\bar{c}\bar{c}$ and fully bottom $bb\bar{b}\bar{b}$ tetraquarks. In Table 9, the masses and widths of all currently observed fully charmed tetraquark states and our candidates for the interpretation of such states are given. One state named X(6900) has already been reliably detected by all three Collaborations (LHCb 2020 [5], CMS 2022 [6], ATLAS 2022 [7]). It is clearly a candidate for the excited fully charmed state. Moreover, the measured value of its mass is very close to our prediction. In fact, we have five candidates for this resonance with the masses within the range of 50 MeV from the measured X(6900) mass. Thus, it is important to measure the quantum numbers of this state(s). Additionally LHCb data indicate two wide and not very distinctive peaks near 6.4 GeV and 7.2 GeV, which can also be interpreted as ground and excited fully charmed tetraquark states.

Table 9. Exotic X states observed by the LHCb [5], CMS [6] and ATLAS [7] Collaborations in di-J/ψ invariant mass spectra and our candidates. All masses are given in MeV.

Collaboration	**State**	**Mass**	**Width**	**Our Candidates**			
				State	S	J^{PC}	**Mass**
ATLAS	X(6200)	$6220 \pm 50^{+40}_{-50}$	$310 \pm 120^{+70}_{-80}$	1S	0	0^{++}	6190
LHCb	X(6400)	≈ 6400		1S	2	2^{++}	6367
CMS	X(6600)	$6552 \pm 10 \pm 12$	$124 \pm 29 \pm 34$	1S	2	2^{++}	6367
				2S	0	0^{++}	6782
ATLAS		$6620 \pm 30^{+20}_{-10}$	$310 \pm 90^{+60}_{-110}$				
LHCb	X(6900)	$6905 \pm 11 \pm 7$	$80 \pm 19 \pm 33$	2S	2	2^{++}	6868
				1D	0	2^{++}	6921
		$6886 \pm 11 \pm 11$	$168 \pm 33 \pm 69$	1D	2	0^{++}	6899
CMS		$6927 \pm 9 \pm 5$	$122 \pm 22 \pm 19$	1D	2	1^{++}	6904
				1D	2	2^{++}	6915
ATLAS		$6870 \pm 30^{+60}_{-10}$	$120 \pm 40^{+30}_{-10}$				
LHCb	X(7200)	≈ 7200		3S	0	0^{++}	7259
ATLAS		$7220 \pm 30^{+20}_{-30}$	$100^{+130+60}_{-70-50}$				
CMS	X(7300)	$7287 \pm 19 \pm 5$	$95 \pm 46 \pm 20$	3S	0	0^{++}	7259
				3S	2	2^{++}	7333

Very recently, the CMS [6] and ATLAS [7] Collaborations reported preliminary results on the observation of exotic charmed states. The CMS Collaboration observed three distinct states in the $J/\psi J/\psi$ mass spectrum: X(6600), X(6900) and X(7300). The ATLAS Collaboration observed four distinct states in the di-J/ψ and $J/\psi + \psi(2S)$ channels: X(6200), X(6600), X(6900) and X(7200). As it was already pointed out before, X(6900) is the most prominent of them all since it was observed by all three experiments with very close mass. The peaking structure around 7.2 GeV in LHCb data was confirmed in these experiments (X(7200) and X(7300)). The X(6200) observed by ATLAS is very close to our prediction for the lowest ground state 0^{++} with the mass 6190 MeV. The authors of Ref. [37] also predicted this state from the analysis of the LHCb data back in 2021. For the X(6600) structure observed both by CMS and ATLAS, we also propose candidates but with greater deviations from central values of the observed mass.

On the other hand, searches for the fully bottom tetraquark in the process

$$pp \longrightarrow X_{bb\bar{b}\bar{b}} \longrightarrow \Upsilon(1S)\Upsilon(1S) \tag{39}$$

in the mass range 17.5–20 GeV (covering the mass range we predict to be 19.3–20 GeV) have not yet yielded any results (LHCb 2018 [10], CMS 2017 [11], 2020 [12]). Moreover, lattice calculations [38] do not find fully bottom tetraquark bound states in this mass region. Such a conclusion correlates with our results that the masses of the fully bottom tetraquarks are significantly higher than the decay thresholds. Thus, these states rapidly fall apart and can appear only as wide, hard-to-detect resonances. However, according to our calculations, there are two states of such tetraquarks, corresponding to high orbital excitations with high values of total spin J that lie below any decay thresholds; these are the states already mentioned in (37) and (38). Therefore, these states can be observed as narrow states decaying to lighter hadrons.

6. Theoretical Predictions

In Tables 10–30, we compare our predictions for the masses (Table 3) with the results of other scientific groups obtained in different theoretical approaches.

We introduced abbreviations in Tables 10–30, but only in cases when the authors used different models or parameter values within the same work. The most common abbreviations are the following.

- DA, MM, mix—diquark–antidiquark, meson–meson models and their mixing;
- $(\text{I-III})_d$—different sets of variable parameter values (quark masses, potential parameters, constants, etc.).

Other abbreviations that occur a few times only are as follows:

- SpB, OscI,II [39]—spherical bag model and oscillating potential model;
- QDCSM, ChQM [40]—quark delocalization color screening model and chiral quark model;
- RSM [41]—real scaling method;
- Cur, Op [42,43]—different expressions for currents;
- LO, NLO, NLO$\oplus$G3 [42,44]—higher corrections;
- CQM, CMIM, MCFTM [45]—constituent quark model, color-magnetic interaction model and multiquark color flux-tube model;
- K [46,47]—other geometric configurations of the system that are neither diquark nor meson;
- NR, Rel [48]—non-relativistic and relativistic considerations, respectively;
- Bt, Fl [49]—"butterfly" and "flip-flop" potentials.

A few more clarifying notes for Tables 10–30 are as follows:

- In many papers using the diquark–antidiquark picture, the cases of color antitriplet-diquark–triplet-antidiquark $\bar{3} \otimes 3$ and color sextet-diquark–antisextet-antidiquark $6 \otimes \bar{6}$ were considered. As we discussed in Section 2, in the color sextet (anti)diquark, the interaction potential between (anti)quarks within the (anti)diquark is repulsive, and thus a corresponding diquark cannot be a bound state, which we consider inappropriate for our problem. Therefore, in Tables 10–30, we give theoretical predictions for the masses calculated only for the $\bar{3} \otimes 3$ configuration. If the results were a mixture of two configurations, we chose those masses that contain more of the triplet state in percentage. We note a general trend: in almost all cases, the calculated masses of sextet configurations turned out to be approximately $10 - 100$ MeV higher than their triplet counterparts.
- In some papers (for example, [50]), tetraquarks containing excited diquarks were also considered. Again, as discussed in Section 2, we have limited ourselves to diquark ground states. Therefore, the masses of such tetraquarks, composed of excited diquarks, are not included in our comparison.
- * in [39] for model 1, corrections were calculated only for all 1S states and for the two lowest 1P states; corrections for all other states were not calculated.
- ** Two cases were considered in [51]: the presence and absence of the heavy η_b-meson exchange. The results only for the case without such an exchange are given.
- *** in [42], LO results were also obtained, but they are quite similar to NLO$\oplus$G3, so we do not present them.
- **** in [44], all results were obtained in two mass schemes: in the $\overline{MS}$-scheme and on-Shell-scheme. In view of the already colossal number of results of this study, we took the masses only in the $\overline{MS}$-scheme.

Table 10. Comparison of theoretical predictions for the masses of the $cc\bar{c}\bar{c}$ tetraquark ground state (1S) with the axialvector diquark and antidiquark. S is the total spin of the diquark–antidiquark system. All masses are given in MeV. Masses are sorted chronologically, oldest predictions first. Our results are given in bold.

$d\bar{d}'$	$A\bar{A}$		
State	**1S**		
S	**0**	**1**	**2**
J^{PC}	$\mathbf{0^{++}}$	$\mathbf{1^{+-}}$	$\mathbf{2^{++}}$
Our	**6190**	**6271**	**6367**
[52]	6200		
[39]	6276 (DA, SpB); 6426 (DA, OscI); 6450 (DA, OscII); 6221, 6260 (MM, SpB)	6276 (DA, SpB); 6440 (DA, OscI); 6450 (DA, OscII); 6221, 6260 (MM, SpB)	6276 (DA, SpB); 6469 (DA, OscI); 6450 (DA, OscII); 6221, 6260 (MM, SpB)
[53]	6477	6528	6573
[54]	6038∼6115	6101∼6176	6172∼6216
[55]	5970	6050	6220
[56]	5966	6051	6223
[57]	5300 ± 500		
[58]	6192 ± 25		
[59]	5990 ± 80		6090 ± 80
[60,61]	6460 ± 160, 6470 ± 160	6510 ± 150	6510 ± 150
[62]	7016	6899	6956
[48]	$\lesssim 6140$		
[63,64]	5969	6021	6115
[65]	6487	6500	6524
[66]	5970 ± 40		
[67]		6050 ± 80	
[68]	6425 (Id); 6483 (IId)	6425 (Id); 6450 (IId)	6432 (Id); 6479 (IId)
[69]	5883	6120	6246
[70]	6192 ± 25		6429 ± 25
[40]	6128, 6270, 6358 (DA, QDCSM (I-III)$_d$); 6466, 6482, 6493 (DA, ChQM (I-III)$_d$); 5961∼6206 (MM, QDCSM (I-III)$_d$); 5961∼6701 (MM, ChQM (I-III)$_d$)	6149, 6285, 6375 (DA, QDCSM (I-III)$_d$); 6479, 6488, 6495 (DA, ChQM (I-III)$_d$); 6079∼6088 (MM, QDCSM (I-III)$_d$); 6079∼6575 (MM, ChQM (I-III)$_d$)	6197, 6314, 6407 (DA, QDCSM (I-III)$_d$); 6498, 6499, 6505 (DA, ChQM (I-III)$_d$); 6197∼6207 (MM, QDCSM (I-III)$_d$); 6197∼6602 (MM, ChQM (I-III)$_d$)
[71]	6542	6515	6543
[50]	6455	6500	6524
[41]	6360 (DA); 5973 (MM); 5973 (mix); 6510 (RSM)	6398 (DA); 6084 (MM); 6084 (mix); 6600 (RSM)	6410 (DA); 6194 (MM); 6194 (mix); 6708 (RSM)
[72]	5960 (Id); 6198 (IId)	6009 (Id); 6246 (IId)	6100 (Id); 6323 (IId)
[42,43]	6450 ± 75 (DA, Cur, NLO⊕G3); 6471 ± 67 (DA, Op, NLO⊕G3); 6029 ± 198, 6376 ± 367, 6494 ± 66, 6675 ± 98 (MM)		
[73]	6469 (DA); 6536, 6657 (MM); 6423, 6650 (mix)	6674 (DA); 6671 (MM); 6627 (mix)	7026 (DA); 7030 (MM); 7014 (mix)
[74]	6351	6441	6471
[75]	6476	6441	6475

Table 10. *Cont.*

$d\bar{d}'$	$A\bar{A}$		
State	**1S**		
S	**0**	**1**	**2**
J^{PC}	0^{++}	1^{+-}	2^{++}
Our	**6190**	**6271**	**6367**
[45]	6573 (CQM); 6035 (CMIM); 6454 (MCFTM)	6580 (CQM); 6139 (CMIM); 6463 (MCFTM)	6607 (CQM); 6194 (CMIM); 6486 (MCFTM)
[76]	6460^{+130}_{-170}		
[77]	6200		
[78]	6520 ± 100	6570 ± 100	6600 ± 100
[79]	6419 (Id); 6390 (IId); 6415 (IIId)	6456 (Id); 6419 (IId); 6454 (IIId)	6516 (Id); 6476 (IId); 6514 (IIId)
[80]	6196		
[81]	6440 ± 110, 6520 ± 110, 6870 ± 110, 6960 ± 110	-	
[82]	6271	6231	6287
[46,47]	6421 (DA); 5936, 6268 (MM); 6150, 6340 (K)	6439 (DA); 6070, 6325 (MM); 6271, 6436 (K)	6472 (DA); 6204, 6338 (MM); 6358, 6473 (K)
[83]	5939	5986	6079
[84]	6498	6481	6502
[85]	6466	6494	6551
[86]	6906	5955 (Id); 6896 (IId)	5960
[87]	6322	6354	6385
[88]	6360^{+180}_{-160}, 6540^{+190}_{-180}	6470^{+180}_{-170}	6520^{+170}_{-170}
[89]	6270 (Id); 6271 (IId); 6201 (IIId)	6424 (Id); 6435 (IId); 6396 (IIId)	6424 (Id); 6435 (IId); 6391 (IIId)
[90]	6055^{+69}_{-74}		6090^{+62}_{-66}
[91]	7438-7542		
[49]	6874 (Bt); 6850 (FL); 6822 (mix)	6913 (Bt); 6870 (FL); 6822 (mix)	6990 (Bt); 6913 (FL); 6822 (mix)
[92]	5978	6155	6263
[44]	6070^{+50}_{-70}, 6070^{+80}_{-100} (DA, LO); 6600^{+90}_{-100}, 6690^{+100}_{-120} (DA, NLO); $5090^{+60}_{-80} \sim 7110^{+130}_{-150}$ (MM, LO); $6360^{+60}_{-100} \sim 8330^{+130}_{-150}$ (MM, NLO)	6080^{+40}_{-100} (DA, LO); 6650^{+100}_{-130} (DA, NLO); $6040^{+60}_{-80} \sim 7070^{+140}_{-160}$ (MM, LO); $6650^{+90}_{-100} \sim 8320^{+180}_{-200}$ (MM, NLO)	6070^{+80}_{-100}, 6150^{+80}_{-100} (DA, LO); 6980^{+90}_{-110}, 7250^{+100}_{-110} (DA, NLO); $6110^{+60}_{-80} \sim 7100^{+130}_{-150}$ (MM, LO); $7030^{+100}_{-120} \sim 8890^{+210}_{-240}$ (MM, NLO)
[93]	6200 ± 100	6240 ± 100	6270 ± 90
[94]	7035, 7202	7050, 7274	7069, 7281
[95]	6384	6452	6483
[96]	6035	6137	6194

Table 11. Same as in Table 10 but for the first orbital excitation (1P). Our results are given in bold.

$d\bar{d}'$	$A\bar{A}$						
State	1P						
S	0		1			2	
J^{PC}	1^{--}	0^{-+}	1^{-+}	2^{-+}	1^{--}	2^{--}	3^{--}
Our	**6631**	**6628**	**6634**	**6644**	**6635**	**6648**	**6664**
[97]	6550	6550	6550	6550	6550	6550	6550
[39]	6694 (OscI); 6714 (OscII)	6695 (OscI); 6714 (OscII)	6718 (OscI); 6714 (OscII)	6718 (OscI); 6714 (OscII)	6718 (OscI); 6714 (OscII)	6718 (OscI); 6714 (OscII)	6718 (OscI); 6714 (OscII)
[53]	7004	6969	7013	7033			
[54]	6998∼7052	6993∼7051	7275∼7363	7002∼7055		7278∼7357	
[98]	6420^{+29}_{-32} (DA); 6411^{+25}_{-43} (MM)						
[60,61]	6830 ± 180	6850 ± 180	6880 ± 180				
[63,64]	6577	6480	6577	6610	6495	6600	6641
[67]	6110 ± 80						
[69]	6580	6596			6584		
[50]	6636	6681	6676	6667	6768	6630	6801
[83]	6553	6460	6554	6587	6459	6577	6623
[84]	6740	6723	6743	6752	6740	6739	6753
[86]	6060 (Id); 6999 (IId)	6054 (Id); 6995 (IId)	6054 (Id); 6995 (IId)	6054 (Id); 6995 (IId)	6056 (Id); 6996 (IId)	6056 (Id); 6996 (IId)	6056 (Id); 6996 (IId)
[88]	6990^{+230}_{-200}, 7170^{+280}_{-220} 6610^{+120}_{-150} (DA, LO);	7000^{+230}_{-200}, 7020^{+240}_{-200} 6540^{+120}_{-140} (DA, LO);	6980^{+210}_{-190}, 7070^{+210}_{-190} 6530^{+110}_{-160} (DA, LO);				
[44]	7970^{+100}_{-170} (DA, NLO); 6530^{+110}_{-140} $\sim 6610^{+120}_{-140}$ (MM, LO); 7550^{+140}_{-150} $\sim 8090^{+60}_{-160}$ (MM, NLO)	7510^{+120}_{-160} (DA, NLO); 6530^{+120}_{-140} $\sim 6560^{+120}_{-150}$ (MM, LO); 7300^{+110}_{-130} $\sim 8530^{+150}_{-190}$ (MM, NLO)	8020^{+80}_{-170} (DA, NLO); 6530^{+110}_{-140} $\sim 6610^{+120}_{-140}$ (MM, LO); 7550^{+140}_{-150} $\sim 8090^{+60}_{-160}$ (MM, NLO)				
[93]	6330 ± 100						

Table 12. Same as in Table 10 but for the first radial excitation (2S). Our results are given in bold.

$d\bar{d}'$	$A\bar{A}$		
State	2S		
S	0	1	2
J^{PC}	0^{++}	1^{+-}	2^{++}
Our	**6782**	**6816**	**6868**
[63,64]	6663	6675	6698
[68]		6856 (Id); 6894 (IId)	6864 (Id); 6919 (IId)
[69]	6573	6669	6739
[70]	6871 ± 25		6967 ± 25
[40]	6950, 6975 (DA, QDCSM (I-III)$_d$); 6825, 6900, 6910 (DA, ChQM (I-III)$_d$)	7250, 7280 (DA, QDCSM (I-III)$_d$); 7250, 7275, 7280 (DA, ChQM (I-III)$_d$)	
[71]	6940	6928	6948
[75]	6908	6896	6921
[99]	6480 ± 80	6520 ± 80	6560 ± 80
[79]	6916 (Id); 6773 (IId); 6924 (IIId)	6957 (Id); 6792 (IId); 6966 (IIId)	7001 (Id); 6843 (IId); 7011 (IIId)
[83]	6642	6654	6676
[84]	7007	6954	6917
[85]	6883	6911	6968
[86]	7073 (Id); 8095 (IId)	7025 (Id); 8060 (IId)	7041 (Id); 8072 (IId)
[87]	6575	6609	6639
[89]	6393 (Id); 6411 (IId); 6575 (IIId)	6458 (Id); 6502 (IId); 6799 (IIId)	6458 (Id); 6502 (IId); 6794 (IIId)
[90]	6555^{+36}_{-37}		6566^{+34}_{-35}
[100]	6908	6919	6927
[93]	6570 ± 90	6640 ± 90	6690 ± 90

Table 13. Same as in Table 10 but for the second orbital excitation (1D). Our results are given in bold.

$d\bar{d}'$	$A\bar{A}$								
State	**1D**								
S	**0**		**1**			**2**			
J^{PC}	2^{++}	1^{+-}	2^{+-}	3^{+-}	0^{++}	1^{++}	2^{++}	3^{++}	4^{++}
Our	**6921**	**6909**	**6920**	**6932**	**6899**	**6904**	**6915**	**6929**	**6945**
[97]	6780	6780	6780	6780	6780	6780	6780	6780	6780
[54]			6586∼6648			6530∼6609			
[60,61]						6340 ± 190			
[69]	6827	6829			6827	6827	6827		
[40]					7140, 7150, 7170 (DA, QDCSM (I-III)$_d$); 7150, 7160 (DA, ChQM (I-III)$_d$)				
[100]	6832	6833	6835	6844	6848	6851	6857	6863	6870
[44]						7040^{+130}_{-150} (DA, LO); 7410^{+230}_{-300} (DA, NLO); $6040^{+60}_{-80} \sim 7070^{+140}_{-160}$ (MM, LO); $6650^{+90}_{-100} \sim 8320^{+180}_{-200}$ (MM, NLO)			

Table 14. Same as in Table 10 but for the first orbital and radial excitation (2P). Our results are given in bold.

$d\bar{d}'$	$A\bar{A}$						
State	**2P**						
S	**0**		**1**			**2**	
J^{PC}	1^{--}	0^{-+}	1^{-+}	2^{-+}	1^{--}	2^{--}	3^{--}
Our	**7091**	**7100**	**7099**	**7098**	**7113**	**7113**	**7112**
[63,64]	6944	6867	6944	6970	6876	6962	6997
[69]	6940	6953			6943		
[99]	6580 ± 90						
[83]	6925	6851	6926	6951	6849	6944	6982
[86]	7143 (Id); 8174 (IId)	7130 (Id); 8162 (IId)	7130 (Id); 8162 (IId)	7130 (Id); 8162 (IId)	7134 (Id); 8166 (IId)	7134 (Id); 8166 (IId)	7134 (Id); 8166 (IId)
[93]	6740 ± 90						

Table 15. Same as in Table 10 but for the second radial excitation (3S). Our results are given in bold.

$dd\bar{d}'$	$A\bar{A}$		
State	**3S**		
S	**0**	**1**	**2**
J^{PC}	$\mathbf{0^{++}}$	$\mathbf{1^{+-}}$	$\mathbf{2^{++}}$
Our	**7259**	**7287**	**7333**
[68]		6915 (Id); 7036 (IId)	6919 (Id); 7058 (IId)
[69]	6948	7016	7071
[40]	7225, 7250 (DA, QDCSM (I-III)$_d$); 7210, 7250, 7260 (DA, ChQM (I-III)$_d$)		
[71]	7063	7052	7064
[75]	7296	7300	7320
[99]	6940 ± 80	6960 ± 80	7000 ± 80
[79]	7224 (Id); 7054 (IId); 7229 (IIId)	7263 (Id); 7066 (IId); 7268 (IIId)	7257 (Id); 7097 (IId); 7258 (IIId)
[83]	7010	7017	7032
[84]		7024	7030
[85]	7225	7253	7310
[87]	6782	6814	6842
[89]	6441 (Id); 6477 (IId); 6897 (IIId)	6464 (Id); 6536 (IId); 7148 (IIId)	6464 (Id); 6536 (IId); 7148 (IIId)
[90]	6883^{+27}_{-27}		6890^{+27}_{-26}
[100]	7240	7243	7248
[93]	6920 ± 90	7030 ± 90	7090 ± 90

Table 16. Same as in Table 10 but for the ground state (1S) of $cb\bar{c}\bar{b}$ composed from the axialvector diquark and antidiquark. Our results are given in bold.

$dd\bar{d}'$	$A\bar{A}$		
State	**1S**		
S	**0**	**1**	**2**
J^{PC}	$\mathbf{0^{++}}$	$\mathbf{1^{+-}}$	$\mathbf{2^{++}}$
Our	**12,838**	**12,855**	**12,883**
[56]	12,471	12,488	12,566
[62]	13,483	13,592	13,590
[48]	$\lesssim 12,620$		
[65]	12,864	12,864	12,884
[101]	12,746 (DA); 12,322, 12,684 (MM); 12,322 (mix)	12,776 (DA); 12,432, 12,737 (MM); 12,432 (mix)	12,809 (DA); 12,561, 12,791 (MM); 12,561 (mix)
[69]	12,374	12,491	12,576
[74]	12,534	12,510	12,582
[45]	13,043 (CQM); 12,354 (CMIM); 12,955 (MCFTM)	13,052 (CQM); 12,436 (CMIM); 12,955 (MCFTM)	13,084 (CQM); 12,548 (CMIM); 12,984 (MCFTM)
[81]	$12,510 \pm 100$, $12,580 \pm 100$, $12,670 \pm 100$, $12,740 \pm 110$	-	
[82]	12,682	12,720	12,755
[46,47]	12,861 (DA); 12,369, 12,809 (MM); 12,599, 12,717 (K)	12,888 (DA); 12,431, 12,843 (MM); 12,635, 12,768 (K)	12,926 (DA); 12,565, 12,885 (MM); 12,771, 12,844 (K)
[102]	$12,460^{+170}_{-150}$	$12,380^{+130}_{-120}$	$12,300^{+150}_{-140}$
[90]	$12,387^{+109}_{-120}$		$12,401^{+117}_{-106}$
[92]	12,503	12,016	12,897
[95]	12,759	12,797	12,882
[96]	12,595	12,573	12,597

Table 17. Same as in Table 10 but for the first orbital excitation (1P) of $cb\bar{c}\bar{b}$ composed from the axialvector diquark and antidiquark. Our results are given in bold.

$d\bar{d}'$	$A\bar{A}$						
State	1P						
S	0		1			2	
J^{PC}	$\mathbf{1^{--}}$	$\mathbf{0^{-+}}$	$\mathbf{1^{-+}}$	$\mathbf{2^{-+}}$	$\mathbf{1^{--}}$	$\mathbf{2^{--}}$	$\mathbf{3^{--}}$
Our	**13,103**	**13,100**	**13,103**	**13,108**	**13,103**	**13,109**	**13,116**
[69]	12,934	12,943			12,944		

Table 18. Same as in Table 10 but for the first radial excitation (2S) of $cb\bar{c}\bar{b}$ composed from the axialvector diquark and antidiquark. Our results are given in bold.

$d\bar{d}'$	$A\bar{A}$		
State	**2S**		
S	**0**	**1**	**2**
J^{PC}	$\mathbf{0^{++}}$	$\mathbf{1^{+-}}$	$\mathbf{2^{++}}$
Our	**13,247**	**13,256**	**13,272**
[69]	12,975	13,022	13,063
[90]	$12,911^{+48}_{-51}$		$12,914^{+49}_{-49}$

Table 19. Same as in Table 10 but for the second orbital excitation (1D) of $cb\bar{c}\bar{b}$ composed from the axialvector diquark and antidiquark. Our results are given in bold.

$d\bar{d}'$	$A\bar{A}$								
State	**1D**								
S	**0**		**1**				**2**		
J^{PC}	$\mathbf{2^{++}}$	$\mathbf{1^{+-}}$	$\mathbf{2^{+-}}$	3^{+-}	$\mathbf{0^{++}}$	$\mathbf{1^{++}}$	$\mathbf{2^{++}}$	$\mathbf{3^{++}}$	$\mathbf{4^{++}}$
Our	**13,306**	**13,299**	**13,304**	**13,311**	**13,293**	**13,296**	**13,301**	**13,308**	**13,317**
[69]	13,166	13,167			13,170	13,168	13,166		

Table 20. Same as in Table 10 but for the first orbital and radial excitation (2P) of $cb\bar{c}\bar{b}$ composed from the axialvector diquark and antidiquark. Our results are given in bold.

$d\bar{d}'$	$A\bar{A}$						
State	**2P**						
S	**0**		**1**			**2**	
J^{PC}	$\mathbf{1^{--}}$	$\mathbf{0^{-+}}$	$\mathbf{1^{-+}}$	$\mathbf{2^{-+}}$	$\mathbf{1^{--}}$	$\mathbf{2^{--}}$	$\mathbf{3^{--}}$
Our	**13,428**	**13,431**	**13,431**	**13,431**	**13,434**	**13,435**	**13,436**
[69]	13,262	13,269			13,269		

Table 21. Same as in Table 10 but for the second radial excitation (3S) of $cb\bar{c}\bar{b}$ composed from the axialvector diquark and antidiquark. Our results are given in bold.

$d\bar{d}'$	$A\bar{A}$		
State	**3S**		
S	**0**	**1**	**2**
J^{PC}	$\mathbf{0^{++}}$	$\mathbf{1^{+-}}$	$\mathbf{2^{++}}$
Our	**13,558**	**13,566**	**13,580**
[69]	13,301	13,335	13,365
[90]	$13,200^{+35}_{-36}$		$13,202^{+35}_{-36}$

Table 22. Same as in Table 10 but for the ground state (1S) first orbital excitation (1P) and first radial excitation (2S) of $cb\bar{c}\bar{b}$ composed from the mixture of axialvector and scalar diquark and antidiquark. Our results are given in bold.

$d\bar{d}'$	$\frac{1}{\sqrt{2}}\left(A\bar{S}\pm S\bar{A}\right)$				
State	**1S**	**1P**			**2S**
S		**1**			
J^{PC}	$1^{+\pm}$	$0^{-\pm}$	$1^{-\pm}$	$2^{-\pm}$	$1^{+\pm}$
Our	**12,863**	**13,096**	**13,099**	**13,104**	**13,257**
[56]	12,485 (+); 12,424 (−)				
[62]	13,599 (+); 13,555 (−)				
[65]	12,870 (+); 12,852 (−)				
[101]	12,804 (DA); 12,561, 12,737 (MM); 12,561 (mix) (+)				
[69]	12,533	12,922	12,922 (−)		13,036
[74]	12,569 (+); 12,510 (−)				
[82]	12,703 (+); 12,744 (−)				
[46,47]	12,903 (DA); 12,431, 12,843 (MM); 12,635, 12,768 (K) (+)				
[102]	$12,300^{+150}_{-140}$ (+); $12,320^{+150}_{-130}$ (−)				
[92]	12,155 (+); 12,896 (−)				
[95]	12,857 (+)				
[96]	12,538 (+); 12,339 (−)				

Table 23. Same as in Table 10 but for the second orbital excitation (1D) first orbital and radial excitation (2P) and second radial excitation (3S) of $cb\bar{c}\bar{b}$ composed from the mixture of axialvector and scalar diquark and antidiquark. Our results are given in bold.

$d\bar{d}'$	$\frac{1}{\sqrt{2}}\left(A\bar{S}\pm S\bar{A}\right)$						
State	**1D**			**2P**			**3S**
S				**1**			
J^{PC}	$1^{+\pm}$	$2^{+\pm}$	$3^{+\pm}$	$0^{-\pm}$	$1^{-\pm}$	$2^{-\pm}$	$1^{+\pm}$
Our	**13,293**	**13,298**	**13,305**	**13,426**	**13,426**	**13,427**	**13,566**
[69]	13,154			13,250	13,250 (−)		13,342

Table 24. Same as in Table 10 but for the ground state (1S), first orbital excitation (1P), first radial excitation (2S), second orbital excitation (1D), first orbital and radial excitation (2P), second radial excitation (3S) of $cb\bar{c}\bar{b}$ composed from the scalar diquark and antidiquark. Our results are given in bold.

$d\bar{d}'$	$S\bar{S}$					
State	**1S**	**1P**	**2S**	**1D**	**2P**	**3S**
S	**0**					
J^{PC}	$\mathbf{0^{++}}$	$\mathbf{1^{--}}$	$\mathbf{0^{++}}$	$\mathbf{2^{++}}$	$\mathbf{1^{--}}$	$\mathbf{0^{++}}$
Our	**12,856**	**13,095**	**13,250**	**13,293**	**13,420**	13,559
[56]	12,359					
[62]	13,553					
[65]	12,835					
[69]	12,521	12,910	13,024	13,143	13,238	13,330
[74]	12,534					
[82]	12,747					
[46,47]	12,892 (DA); 12,369, 12,809 (MM); 12,599, 12,717 (K)					
[102]	$12,280^{+150}_{-140}$					
[92]	12,359					
[96]	12,431					

Table 25. Same as in Table 10 but for the ground state (1S) of the $bb\bar{b}\bar{b}$. Our results are given in bold.

$d\bar{d}'$	$A\bar{A}$		
State	**1S**		
S	**0**	**1**	**2**
J^{PC}	$\mathbf{0^{++}}$	$\mathbf{1^{+-}}$	$\mathbf{2^{++}}$
Our	**19,314**	**19,320**	**19,330**
[56]	18,754	18,808	18,916
[58]	$18,826 \pm 25$		
[59]	$18,840 \pm 90$		$18,850 \pm 90$
[60,61]	$18,460 \pm 140$, $18,490 \pm 160$	$18,540 \pm 150$	$18,530 \pm 150$
[103]	18,800		
[62]	20,275	20,212	20,243
[48]	$18,720 \pm 20$ (NR, MM); $18,750 \pm 50$ (Rel, DA); $\lesssim 18,890$		
[38]	$> 18,798$	$> 18,859$	$> 18,921$
[65]	19,322	19,329	19,341
[51]	19,191, 19,221 (DA); 18,670, 18,928, 19,195, 19,205 (MM); 18,670 (mix)	19,227 (DA); 18,799, 19,179 (MM); 18,799 (mix)	19,238 (DA); 18,928, 19,195 (MM); 18,928 (mix)
[66]	$18,690 \pm 30$		
[67]		$18,840 \pm 90$	
[68]	19,247 (Id); 19,305 (IId)	19,247 (Id); 19,311 (IId)	19,249 (Id); 19,325 (IId)
[69]	18,748	18,828	18,900
[70]	$18,826 \pm 25$		$18,956 \pm 25$

Table 25. *Cont.*

$d\bar{d}'$	$A\bar{A}$		
State	**1S**		
S	**0**	**1**	**2**
J^{PC}	0^{++}	1^{+-}	2^{++}
Our	**19,314**	**19,320**	**19,330**
[40]	19,165, 19,256, 19,344 (DA, QDCSM (I-III)$_d$); 19,313, 19,456, 19,466 (DA, ChQM (I-III)$_d$); 18,800∼18,925 (MM, QDCSM (I-III)$_d$); 18,800∼20,041 (MM, ChQM (I-III)$_d$)	19,184, 19,264, 19,354 (DA, QDCSM (I-III)$_d$); 19,323, 19,461, 19,467 (DA, ChQM (I-III)$_d$); 18,860∼18,864 (MM, QDCSM (I-III)$_d$); 18,860∼19,927 (MM, ChQM (I-III)$_d$)	19,236, 19,279, 19,374 (DA, QDCSM (I-III)$_d$); 19,344, 19,471 (DA, ChQM (I-III)$_d$); 18,921∼18,925 (MM, QDCSM (I-III)$_d$); 18,921∼19,933 (MM, ChQM (I-III)$_d$)
[71]	19,255	19,251	19,262
[50]	19,306	19,329	19,341
[72]	18,723 (Id); 18,754 (IId)	18,738 (Id); 18,768 (IId)	18,768 (Id); 18,797 (IId)
[42,43]	$19,872 \pm 156$ (DA, Cur, NLO⊕G3); $19,717 \pm 118$ (DA, Op, NLO⊕G3); $19,259 \pm 88$, $19,430 \pm 145$, $19,770 \pm 137$, $19,653 \pm 131$ (MM)		
[73]	17,975, 19,033 (DA); 17,999, 18,038, 19,036, 19,069 (MM); 17,917, 18,010, 19,280 (mix)	18065, 19,093 (DA); 18,062, 19,087 (MM); 18,009, 19,338, 19,627 (mix)	18,241, 19,211 (DA); 18,238, 19,207 (MM); 18,189, 19,451, 19,708 (mix)
[74]	19,199	19,276	19,289
[75]	19,226	19,214	19,232
[45]	19,417 (CQM); 18,834 (CMIM); 19,377 (MCFTM)	19,413 (CQM); 18,890 (CMIM); 19,373 (MCFTM)	19,429 (CQM); 18,921 (CMIM); 19,387 (MCFTM)
[104]	19,650, 20,110, 21,470 (Id); 22,310, 22,660, 23,720 (IId)		
[79]	19,205 (Id); 19,187 (IId); 19,209 (IIId)	19,221 (Id); 19,202 (IId); 19,225 (IIId)	19,253 (Id); 19,234 (IId); 19,257 (IIId)
[80]	18,572		
[81]	$18,380 \pm 110$, $18,440 \pm 100$, $18,500 \pm 100$, $18,590 \pm 110$	-	
[82]	18,981	18,969	19,000
[46,47]	19,196 (DA); 18,802, 19,144 (MM); 18,977, 19,143 (K)	19,205 (DA); 18,864, 19,126 (MM); 19,053, 19,206 (K)	19,223 (DA); 18,926, 19,197 (MM); 19,093, 19,225 (K)
[105]	18,719 (Id); 18,749 (IId)	18,734 (Id); 18,764 (IId)	18,764 (Id); 18,792 (IId)
[87]	19,666	19,673	19,680
[88]	$18,130^{+130}_{-90}$, $18,150^{+140}_{-100}$	$18,140^{+140}_{-90}$	$18,150^{+140}_{-190}$
[89]	19,429 (Id); 19,428 (IId); 19,302 (IIId)	19,557 (Id); 19,558 (IId); 19,409 (IIId)	19,557 (Id); 19,558 (IId); 19,409 (IIId)
[90]	$18,475^{+151}_{-169}$		$18,483^{+149}_{-168}$
[49]	18,444 (Bt); 18,440 (FL); 18,440 (mix)	18,444 (Bt); 18,440 (FL); 18,440 (mix)	18,444 (Bt); 18,440 (FL); 18,440 (mix)

Table 25. *Cont.*

$d\bar{d}'$	$A\bar{A}$		
State	**1S**		
S	**0**	**1**	**2**
J^{PC}	0^{++}	1^{+-}	2^{++}
Our	**19,314**	**19,320**	**19,330**
[92]	18,752	18,805	18,920
[44]	$18,500^{+170}_{-260}$, $18,510^{+170}_{-260}$ (DA, LO); $18,970^{+50}_{-110}$ (DA, NLO); $18,500^{+170}_{-260} \sim 19,210^{+200}_{-260}$ (MM, LO); $18,930^{+90}_{-160} \sim 19660^{+50}_{-100}$ (MM, NLO)	$18,500^{+170}_{-250}$ (DA, LO); $18,970^{+60}_{-110}$ (DA, NLO); $18,500^{+170}_{-260} \sim 19,210^{+200}_{-260}$ (MM, LO); $18,600^{+190}_{-260} \sim 19,530^{+110}_{-170}$ (MM, NLO)	$18,500^{+170}_{-260}$ (DA, LO); $18,910^{+110}_{-180}$, $18,950^{+70}_{-130}$ (DA, NLO); $18,500^{+170}_{-260} \sim 19,210^{+200}_{-260}$ (MM, LO); $18,890^{+110}_{-180} \sim 19,620^{+40}_{-80}$ (MM, NLO)
[95]	19,240	19,304	19,328
[96]	18,834	18,890	18,921

Table 26. Same as in Table 10 but for the first orbital excitation (1P) of the $bb\bar{b}\bar{b}$. Our results are given in bold.

$d\bar{d}'$	$A\bar{A}$						
State	**1P**						
S	**0**		**1**			**2**	
J^{PC}	1^{--}	0^{-+}	1^{-+}	2^{-+}	1^{--}	2^{--}	3^{--}
Our	**19,536**	**19,533**	**19,535**	**19,539**	**19,534**	**19,538**	**19,545**
[60,61]	$18,770 \pm 160$	$18,790 \pm 180$	$18,830 \pm 180$				
[67]	$18,890 \pm 90$						
[69]	19,281	19,288			19,288		
[50]	19,479	19,500	19,496	19,492	19,603	19,476	19,617
[105]	19,381 (Id); 19,361 (IId)	19,340 (Id); 19,327 (IId)	19,380 (Id); 19,361 (IId)	19,395 (Id); 19,373 (IId)	19,338 (Id); 19,325 (IId)	19,390 (Id); 19,369 (IId)	19,412 (Id); 19,388 (IId)
[88]	$18,460^{+150}_{-110}$	$18,450^{+150}_{-110}$, $18,540^{+160}_{-120}$	$18,560^{+160}_{-110}$, $18,790^{+180}_{-130}$				
[44]	$18,860^{+190}_{-260}$ (DA, LO); $19,180^{+130}_{-200}$ (DA, NLO); $18,850^{+200}_{-260} \sim 18,870^{+190}_{-260}$ (MM, LO); $19,220^{+50}_{-110} \sim 19,310^{+40}_{-90}$ (MM, NLO)	$18,860^{+190}_{-240}$ (DA, LO); $19,230^{+80}_{-140}$ (DA, NLO); $18,850^{+190}_{-260} \sim 18,860^{+190}_{-260}$ (MM, LO); $19,180^{+110}_{-180} \sim 19,310^{+40}_{-90}$ (MM, NLO)	$18,860^{+190}_{-260}$ (DA, LO); $19,230^{+70}_{-130}$ (DA, NLO); $18,850^{+200}_{-260} \sim 18,870^{+190}_{-260}$ (MM, LO); $19,220^{+50}_{-110} \sim 19,310^{+40}_{-90}$ (MM, NLO)				

Table 27. Same as in Table 10 but for the first radial excitation (2S) of the $bb\bar{b}\bar{b}$. Our results are given in bold.

$d\bar{d}'$	$A\bar{A}$		
State	**2S**		
S	**0**	**1**	**2**
J^{PC}	$\mathbf{0^{++}}$	$\mathbf{1^{+-}}$	$\mathbf{2^{++}}$
Our	**19,680**	**19,682**	**19,687**
[68]		19,594 (Id); 19,813 (IId)	19,596 (Id); 19,823 (IId)
[69]	19,335	19,366	19,398
[70]	$19,434 \pm 25$		$19,481 \pm 25$
[71]	19,625	19,625	19,633
[75]	19,583	19,582	19,594
[79]	19,636 (Id); 19,544 (IId); 19,646 (IIId)	19,662 (Id); 19565 (IId); 19,671 (IIId)	19,684 (Id); 19,591 (IId); 19,694 (IIId)
[105]	19,441 (Id); 19,414 (IId)	19,443 (Id); 19,416 (IId)	19,448 (Id); 19,421 (IId)
[87]	19,841	19,849	19,855
[89]	19,512 (Id); 19,515 (IId); 19,591 (IIId)	19,587 (Id); 19,597 (IId); 19,728 (IIId)	19,587 (Id); 19,597 (IId); 19,728 (IIId)
[90]	$19,073^{+59}_{-63}$		$19,075^{+59}_{-62}$
[100]	19,719	19,722	19,726

Table 28. Same as in Table 10 but for the second orbital excitation (1D) of the $bb\bar{b}\bar{b}$. Our results are given in bold.

$d\bar{d}'$	$A\bar{A}$								
State	**1D**								
S	**0**		**1**				**2**		
J^{PC}	$\mathbf{2^{++}}$	$\mathbf{1^{+-}}$	$\mathbf{2^{+-}}$	$\mathbf{3^{+-}}$	$\mathbf{0^{++}}$	$\mathbf{1^{++}}$	$\mathbf{2^{++}}$	$\mathbf{3^{++}}$	$\mathbf{4^{++}}$
Our	**19,715**	**19,710**	**19,714**	**19,720**	**19,705**	**19,707**	**19,711**	**19,717**	**19,724**
[60,61]						$18,320 \pm 180$			
[69]	19,510	19,511			19,513	19,512	19,510		
[100]	19,669	19,671	19,672	19,675	19,677	19,678	19,680	19,684	19,686
[44]						$19,200^{+200}_{-260}$ (DA, LO); $18,850^{+190}_{-260}$ (DA, NLO); $18,500^{+170}_{-260} \sim 19,210^{+200}_{-260}$ (MM, LO); $18,600^{+190}_{-260} \sim 19,530^{+110}_{-170}$ (MM, NLO)			

Table 29. Same as in Table 10 but for the second orbital and radial excitation (2P) of the $bb\bar{b}\bar{b}$. Our results are given in bold.

$d\bar{d}'$	$A\bar{A}$						
State	**2P**						
S	0	**1**			**2**		
J^{PC}	1^{--}	0^{-+}	1^{-+}	2^{-+}	1^{--}	2^{--}	3^{--}
Our	**19,820**	**19,821**	**19,821**	**19,822**	**19,823**	**19,823**	**19,824**
[69]	19,597	19,602			19,602		

Table 30. Same as in Table 10 but for the third radial excitation (3S) of the $bb\bar{b}\bar{b}$. Our results are given in bold.

$d\bar{d}'$	$A\bar{A}$		
State	**3S**		
S	**0**	**1**	**2**
J^{PC}	0^{++}	1^{+-}	2^{++}
Our	**19,941**	**19,943**	**19,947**
[68]		19,681 (Id); 20,065 (IId)	19,682 (Id); 20,077 (IID)
[69]	19,644	19,665	19,688
[71]	19,726	19,733	19,736
[75]	19,887	19,889	19,898
[79]	19,907 (Id); 19,795 (IId); 19,913 (IIId)	19,930 (Id); 19,815(IId); 19,936 (IIId)	19,926 (Id); 19,822 (IId); 19,930 (IIId)
[105]	19,759 (Id); 19,701 (IId)	19,760 (Id); 19,703 (IId)	19,764 (Id); 19,706 (IId)
[87]	20,001	20,012	20,021
[89]	19,557 (Id); 19,565 (IId); 19,845 (IIId)	19,597 (Id); 19,615 (IId); 20,016 (IIId)	19,597 (Id); 19,615 (IId); 20,016 (IIId)
[90]	$19,353^{+42}_{-42}$		$19,355^{+41}_{-43}$
[100]	19,979	19,980	19,982

We compare our predictions with the results obtained in the following approaches and models:

- Various quark models: [39–41,45–58,62–66,68–75,77,79,80,82–87,89–92,94–97,100,101,103–105].
- QCD sum rules: [42–44,59–61,67,76,78,81,88,93,99,102].
- Lattice calculations: [38,98].

Among them, the following configurations can be distinguished:

- Diquark–antidiquark model: [38–42,44–51,55,56,58–74,76,78–80,82–85,87,89,90,92–103,105].
- Meson–meson model: [39–42,44,46,47,51,73,81,86,88,94,98,101].
- Mixing of the diquark and meson structures: [41,51,57,73,75,101].

It is seen from Tables 10–30 that our results agree well (within the ±50 MeV range) with the following results:

- For the $cc\bar{c}\bar{c}$ tetraquark:
  - In the diquark–antidiquark picture: [48,58,72,77,80] (all predictions); [70,89,93] (ground states only); [50,60,61,69] (1P); [68] (2S); [85,100] (3S); [40] (1S, 3S); [79] (2S, 3S); [44] (1P, 1D).
  - In the other models: [40,42–44,46,47,52,77] (all predictions); [39,88] (ground states only); [86] (2P); [75] (3S).
- For the $cb\bar{c}\bar{b}$ tetraquark:
  - In the diquark–antidiquark picture: $A\bar{A}$, $\frac{1}{\sqrt{2}}(A\bar{S} \pm S\bar{A})$, $S\bar{S}$ – [46,47,65,95] (all predictions).
  - In other models: $A\bar{A}$ – [46,47,81] (all predictions); $\frac{1}{\sqrt{2}}(A\bar{S} \pm S\bar{A})$, $S\bar{S}$ – [46,47] (all predictions).

- For the $bb\bar{b}\bar{b}$ tetraquark:
  - In the diquark–antidiquark picture: [40,45,50,65,74,95,100] (all predictions); [68] (ground states only); [71] (2S); [79] (2S, 3S).
  - In other models: [40,42,43,73] (all predictions); [44] (ground states only); [75] (3S).

A number of other conclusions can be drawn from this data:

- Predictions of Refs. [46,47] are in full agreement with our results for the $cb\bar{c}\bar{b}$ tetraquark;
- Predictions of Refs. [65,95] give good agreement for the $cb\bar{c}\bar{b}$ and $bb\bar{b}\bar{b}$ tetraquarks, but do not agree at all for the $cc\bar{c}\bar{c}$ tetraquark;
- Predictions of Refs. [40,50,68,79,100] give partial agreement for the $cc\bar{c}\bar{c}$ and $bb\bar{b}\bar{b}$ tetraquarks in the diquark–antidiquark picture;
- Predictions of Refs. [40,42–44,75] give partial agreement for the $cc\bar{c}\bar{c}$ and $bb\bar{b}\bar{b}$ tetraquarks in models other than diquark–antidiquark.

In addition, throughout comparison of our results with those of other scientific groups, the following is shown:

- For the $cc\bar{c}\bar{c}$ tetraquark, our results are generally median: there are many results giving both heavier and lighter masses;
- For the $cb\bar{c}\bar{b}$ tetraquark masses, our results exceed those of other scientific groups for all diquark spins and excitations;
- For the $bb\bar{b}\bar{b}$ tetraquark masses, our results are slightly higher than those of most other scientific groups.

The generally higher values of tetraquark masses predicted in our model originate primarily from taking into account the finite size of the diquark. It results in the weakening of the one-gluon exchange potential and, thus, increasing the tetraquark mass.

Note that the authors of Ref. [62] came to unexpected conclusions. They argue that the ground state of the asymmetric tetraquark $bb\bar{c}\bar{b}$ may be stable (its ground states were studied by us in Refs. [14,15] and were found to be significantly above the fall-apart decay thresholds), and they also expect the $cb\bar{c}\bar{b}$ tetraquark to be a narrow state in contradiction with our conclusions.

7. Conclusions

Within the framework of the relativistic quark model, we calculated masses of the ground states, radial (up to 3S) and orbital (up to 1D) excitations of the fully charmed $cc\bar{c}\bar{c}$, doubly charmed-bottom $cb\bar{c}\bar{b}$ and fully bottom $bb\bar{b}\bar{b}$ tetraquarks. An important feature of our calculations is the consistent account of the relativistic effects and the finite size of the diquark (as it is shown in the Section 3), which leads to the weakening of the one-gluon exchange potential due to the form factors of the diquark–gluon interaction.

A detailed analysis of the calculated mass spectra was carried out. We compared calculated tetraquark masses with the thresholds of the strong fall-apart decays into the meson pairs. As shown in Section 5, most of the tetraquark states lie significantly above the meson pair decay threshold. However, tetraquark states with the smallest widths and, as a result, with the most probability to be observed as narrow states, were identified. An argument is given as to why the excited states in general can be narrow, despite the large phase space.

It should be noted that the mass of the narrow state X(6900) recently discovered in the di-J/ψ pair production (LHCb 2020 [5], CMS 2022 [6], ATLAS 2022 [7]) agrees well with our prediction for the masses of the fully charmed tetraquark excited (2S, 1D) states. According to the calculations, several candidates for the interpretation of this state are proposed. Candidates are also identified for all other recently discovered states, such as X(6200) (ATLAS), X(6400) (LHCb), X(6600) (CMS, ATLAS), X(7200) (LHCb, ATLAS), X(7300) (CMS).

In conclusion, we note that experimental searches for fully heavy tetraquarks are currently ongoing and should be continued. Therefore, it can be expected that new experimental candidates will appear in the near future.

Author Contributions: Authors contributed equally to the preparation of the manuscript. Investigation, V.O.G. and E.M.S.; Writing—original draft, V.O.G. and E.M.S.; Writing—review and editing, R.N.F., V.O.G. and E.M.S. All authors have read and agreed to the published version of the manuscript.

Funding: The work of Elena M. Savchenko was funded in part by the Foundation for the Advancement of Theoretical Physics and Mathematics "BASIS" grant number 22-2-10-3-1.

Data Availability Statement: Not applicable.

Acknowledgments: The authors are grateful to D. Ebert for very fruitful and pleasant collaboration in developing the diquark–antidiquark model of tetraquarks. We are grateful to A.V. Berezhnoy for useful discussions.

Conflicts of Interest: The authors declare no conflict of interest.

References

1. Choi, S.K.; Olsen, S.L.; Abe, K.; Abe, T.; Adachi, I.; Ahn, B.S.; Aihara, H.; Akai, K.; Akatsu, M.; Akemoto, M. et al. Observation of a Narrow Charmoniumlike State in Exclusive $B^{\pm} \to K^{\pm}\pi^{+}\pi^{-}J/\psi$ Decays. *Phys. Rev. Lett.* **2003**, *91*, 262001. [CrossRef] [PubMed]
2. Workman, R.L.; Burkert, V.D.; Crede, V.; Klempt, E.; Thoma, U.; Tiator, L.; Agashe, K.; Aielli, G.; Allanach, B.C.; Amsler, C. et al. Review of Particle Physics. *Prog. Theor. Exp. Phys.* **2022**, *2022*, 083C01. [CrossRef]
3. Tornqvist, N.A. Isospin breaking of the narrow charmonium state of Belle at 3872 MeV as a deuson. *Phys. Lett. B* **2004**, *590*, 209–215. [CrossRef]
4. Aaij, R.; Adeva, B.; Adinolfi, M.; Affolder, A.; Ajaltouni, Z.; Albrecht, J.; Alessio, F.; Alexander, M.; Ali, S.; Alkhazov, G. et al. Observation of the Resonant Character of the $Z(4430)^{-}$ State. *Phys. Rev. Lett.* **2014**, *112*, 222002. [CrossRef]
5. Aaij, R.; Abellán Beteta. C.; Ackernley, T.; Adeva, B.; Adinolfi, M.; Afsharnia, H.; Aidala, C.A.; Aiola, S.; Ajaltouni, Z.; Akar, S. et al. Observation of structure in the J/ψ-pair mass spectrum. *Sci. Bull.* **2020**, *65*, 1983–1993. [CrossRef]
6. The CMS Collaboration. *Observation of New Structures in the $J/\psi J/\psi$ Mass Spectrum in pp Collisions at $\sqrt{s} = 13$ TeV, CMS-PAS-BPH-21-003;* Technical report; CERN: Geneva, Switzerland, 2022.
7. The ATLAS Collaboration. *Observation of an Excess of Di-Charmonium Eventsin the Four-Muon Final State with the ATLAS Detector, ATLAS-CONF-2022-040;* Technical report; CERN: Geneva, Switzerland, 2022.
8. Aaij, R.; Adeva, B.; Adinolfi, M.; Affolder, A.; Ajaltouni, Z.; Akar, S.; Albrecht, J.; Alessio, F.; Alexander, M.; Ali, S. et al. Observation of $J/\psi p$ Resonances Consistent with Pentaquark States in $\Lambda_b^0 \to J/\psi K^{-} p$ Decays. *Phys. Rev. Lett.* **2015**, *115*, 072001. [CrossRef]
9. Chen, H.X.; Chen, W.; Liu, X.; Liu, Y.R.; Zhu, S.L. An updated review of the new hadron states. *arXiv* **2022**, arXiv:2204.02649.
10. Aaij, R.; Adeva, B.; Adinolfi, M.; Aidala, C.A.; Ajaltouni, Z.; Akar, S.; Albicocco, P.; Albrecht, J.; Alessio, F.; Alexander, M. et al. Search for beautiful tetraquarks in the Υ(1S)$\mu^{+}\mu^{-}$ invariant-mass spectrum. *J. High Energy Phys.* **2018**, *2018*, 086. [CrossRef]
11. Khachatryan, V.; Sirunyan, A. M.; Tumasyan, A.; Adam, W.; Asilar, E.; Bergauer, T.; Brandstetter, J.; Brondolin, E.; Dragicevic, M.; Erö, J.; et al. Observation of $\Upsilon(1S)$ pair production in proton-proton collisions at $\sqrt{s} = 8$ TeV. *J. High Energy Phys.* **2017**, *05*, 013. [CrossRef]
12. Sirunyan, A.M.; Tumasyan, A.; Adam, W.; Ambrogi, F.; Bergauer, T.; Dragicevic, M.; Erö, J.; Escalante Del Valle, A.; Flechl, M.; Frühwirth, R.; et al. Measurement of the $\Upsilon(1S)$ pair production cross section and search for resonances decaying to Υ(1S)$\mu^{+}\mu^{-}$ in proton-proton collisions at $\sqrt{s} = 13$ TeV. *Phys. Lett. B* **2020**, *808*, 135578. [CrossRef]
13. Bigi, I.; Dokshitzer, Y.; Khoze, V.; Kühn, J.; Zerwas, P. Production and decay properties of ultra-heavy quarks. *Phys. Lett. B* **1986**, *181*, 157–163. [CrossRef]
14. Faustov, R.N.; Galkin, V.O.; Savchenko, E.M. Masses of the $QQ\bar{Q}\bar{Q}$ tetraquarks in the relativistic diquark-antidiquark picture. *Phys. Rev. D* **2020**, *102*, 114030. [CrossRef]
15. Faustov, R.N.; Galkin, V.O.; Savchenko, E.M. Heavy Tetraquarks in the Relativistic Quark Model. *Universe* **2021**, *7*, 94. [CrossRef]
16. Ebert, D.; Faustov, R.N.; Galkin, V.O. Masses of heavy baryons in the relativistic quark model. *Phys. Rev. D* **2005**, *72*, 034026. [CrossRef]
17. Ebert, D.; Faustov, R.N.; Galkin, V.O. Spectroscopy and Regge trajectories of heavy baryons in the relativistic quark-diquark picture. *Phys. Rev. D* **2011**, *84*, 014025. [CrossRef]
18. Logunov, A.A.; Tavkhelidze, A.N. Quasi-Optical Approach in Quantum Field Theory. *Nuovo Cim.* **1963**, *29*, 380–399. [CrossRef]
19. Martynenko, A.P.; Faustov, R.N. Relativistic reduced mass and quasipotential equation. *Theor. Math. Phys.* **1985**, *64*, 765–770. [CrossRef]
20. Galkin, V.O.; Faustov, R.N. Some properties of the solutions of a quasipotential equation. *Theor. Math. Phys.* **1990**, *85*, 1119–1123. [CrossRef]
21. Ebert, D.; Faustov, R.N.; Galkin, V.O.; Martynenko, A.P. Mass spectra of doubly heavy baryons in the relativistic quark model. *Phys. Rev. D* **2002**, *66*, 014008. [CrossRef]
22. Ebert, D.; Faustov, R.N.; Galkin, V.O. Masses of heavy tetraquarks in the relativistic quark model. *Phys. Lett. B* **2006**, *634*, 214–219. [CrossRef]
23. Simonov, Y.A. Perturbation theory in the nonperturbative QCD vacuum. *Phys. Atom. Nucl.* **1995**, *58*, 107–123. [CrossRef]
24. Badalian, A.M.; Veselov, A.I.; Bakker, B.L.G. Restriction on the strong coupling constant in the IR region from the 1D-1P splitting in bottomonium. *Phys. Rev. D* **2004**, *70*, 016007. [CrossRef]
25. Galkin, V.O.; Mishurov, A.Y.; Faustov, R.N. Meson masses in the relativistic quark model. *Sov. J. Nucl. Phys.* **1992**, *55*, 1207–1213.
26. Ebert, D.; Faustov, R.N.; Galkin, V.O.; Lucha, W. Masses of tetraquarks with two heavy quarks in the relativistic quark model. *Phys. Rev. D* **2007**, *76*, 114015. [CrossRef]
27. Faustov, R. Magnetic Moment of the Relativistic Composite System. *Nuovo Cim. A* **1970**, *69*, 37–46. [CrossRef]

28. Faustov, R.N. Relativistic Wavefunction and Form Factors of the Bound System. *Ann. Phys.* **1973**, *78*, 176–189. [CrossRef]
29. Galkin, V.O.; Faustov, R.N. Relativistic corrections to radiative decay widths of vector mesons. *Sov. J. Nucl. Phys.* **1986**, *44*, 1575–1581.
30. Galkin, V.O.; Mishurov, A.Y.; Faustov, R.N. Radiative E1 decays of quarkonium in the framework of relativistic quark model. *Sov. J. Nucl. Phys.* **1990**, *51*, 705–710.
31. Faustov, R.N.; Galkin, V.O. Heavy quark $1/m_Q$ expansion of meson weak decay form-factors in the relativistic quark model. *Z Phys. C* **1995**, *66*, 119–127. [CrossRef]
32. Bugg, D.V. How resonances can synchronise with thresholds. *J. Phys. G: Nucl. Part. Phys.* **2008**, *35*, 075005. [CrossRef]
33. Gasser, J.; Lyubovitskij, V.E.; Rusetsky, A. Hadronic atoms in QCD + QED. *Phys. Rep.* **2008**, *456*, 167–251. [CrossRef]
34. Vijande, J.; Barnea, N.; Valcarce, A. Hyperspherical harmonic study of identical-flavor four-quark systems. *Nucl. Phys. A* **2007**, *790*, 542–545. [CrossRef]
35. Richard, J.M.; Valcarce, A.; Vijande, J. String dynamics and metastability of all-heavy tetraquarks. *Phys. Rev. D* **2017**, *95*, 054019. [CrossRef]
36. Richard, J.M.; Valcarce, A.; Vijande, J. Hall-Post inequalities: Review and application to molecules and tetraquarks. *Ann. Phys.* **2020**, *412*, 168009. [CrossRef]
37. Dong, X.K.; Baru, V.; Guo, F.K.; Hanhart, C.; Nefediev, A. Coupled-Channel Interpretation of the LHCb Double-J/ψ Spectrum and Hints of a New State Near the $J/\psi J/\psi$ Threshold. *Phys. Rev. Lett.* **2021**, *126*, 132001. Erratum in *Phys. Rev. Lett.* **2021**, *127*, 119901. [CrossRef] [PubMed]
38. Hughes, C.; Eichten, E.; Davies, C.T.H. Searching for beauty-fully bound tetraquarks using lattice nonrelativistic QCD. *Phys. Rev. D* **2018**, *97*, 054505. [CrossRef]
39. Ader, J.P.; Richard, J.M.; Taxil, P. Do narrow heavy multiquark states exist? *Phys. Rev. D* **1982**, *25*, 2370. [CrossRef]
40. Jin, X.; Xue, Y.; Huang, H.; Ping, J. Full-heavy tetraquarks in constituent quark models. *Eur. Phys. J. C* **2020**, *80*, 1083. [CrossRef]
41. Chen, X. Fully-charm tetraquarks: $cc\bar{c}\bar{c}$. *arXiv* **2020**, arXiv:2001.06755.
42. Albuquerque, R.M.; Narison, S.; Rabemananjara, A.; Rabetiarivony, D.; Randriamanatrika, G. Doubly-hidden scalar heavy molecules and tetraquarks states from QCD at NLO. *Phys. Rev. D* **2020**, *102*, 094001. [CrossRef]
43. Albuquerque, R.M.; Narison, S.; Rabetiarivony, D.; Randriamanatrika, G. Doubly hidden 0^{++} molecules and tetraquarks states from QCD at NLO. *Nucl. Part. Phys. Proc.* **2021**, *312*, 15289. [CrossRef]
44. Wu, R.H.; Zuo, Y.S.; Wang, C.Y.; Meng, C.; Ma, Y.Q.; Chao, K.T. NLO results with operator mixing for fully heavy tetraquarks in QCD sum rules. *arXiv* **2022**, arXiv:2201.11714.
45. Deng, C.; Chen, H.; Ping, J. Towards the understanding of fully-heavy tetraquark states from various models. *Phys. Rev. D* **2021**, *103*, 014001. [CrossRef]
46. Yang, G.; Ping, J.; Segovia, J. Exotic resonances of fully-heavy tetraquarks in a lattice-QCD insipired quark model. *Phys. Rev. D* **2021**, *104*, 014006. [CrossRef]
47. Yang, G.; Ping, J.; He, L.; Wang, Q. Potential model prediction of fully-heavy tetraquarks $QQ\bar{Q}\bar{Q}$ ($Q = c, b$). *arXiv* **2021**, arXiv:2006.13756..
48. Anwar, M.N.; Ferretti, J.; Guo, F.K.; Santopinto, E.; Zou, B.S. Spectroscopy and decays of the fully-heavy tetraquarks. *Eur. Phys. J. C* **2018**, *78*, 647. [CrossRef]
49. Asadi, Z.; Boroun, G.R. Masses of fully heavy tetraquark states from a four-quark static potential model. *Phys. Rev. D* **2022**, *105*, 014006. [CrossRef]
50. liu, M.S.; Liu, F.X.; Zhong, X.H.; Zhao, Q. Full-heavy tetraquark states and their evidences in the LHCb $di-J/\psi$ spectrum. *arXiv***2020**, arXiv:2006.11952.
51. Chen, X. Analysis of hidden-bottom $bb\bar{b}\bar{b}$ states. *Eur. Phys. J. A* **2019**, *55*, 106. [CrossRef]
52. Iwasaki, Y. A Possible Model for New Resonances – Exotics and Hidden Charm. *Prog. Theor. Phys.* **1975**, *54*, 492. [CrossRef]
53. Lloyd, R.J.; Vary, J.P. All-charm tetraquarks. *Phys. Rev. D* **2004**, *70*, 014009. [CrossRef]
54. Barnea, N.; Vijande, J.; Valcarce, A. Four-quark spectroscopy within the hyperspherical formalism. *Phys. Rev. D* **2006**, *73*, 054004. [CrossRef]
55. Berezhnoy, A.V.; Likhoded, A.K.; Luchinsky, A.V.; Novoselov, A.A. Production of J/ψ-meson pairs and $4c$ tetraquark at the LHC. *Phys. Rev. D* **2011**, *84*, 094023. [CrossRef]
56. Berezhnoy, A.V.; Luchinsky, A.V.; Novoselov, A.A. Heavy tetraquarks production at the LHC. *Phys. Rev. D* **2012**, *86*, 034004. [CrossRef]
57. Heupel, W.; Eichmann, G.; Fischer, C.S. Tetraquark bound states in a Bethe–Salpeter approach. *Phys. Lett. B* **2012**, *718*, 545–549. [CrossRef]
58. Karliner, M.; Nussinov, S.; Rosner, J.L. $QQ\bar{Q}\bar{Q}$ states: Masses, production, and decays. *Phys. Rev. D* **2017**, *95*, 034011. [CrossRef]
59. Wang, Z.G. Analysis of the $QQ\bar{Q}\bar{Q}$ tetraquark states with QCD sum rules. *Eur. Phys. J. C* **2017**, *77*, 432. [CrossRef]
60. Chen, W.; Chen, H.X.; Liu, X.; Steele, T.G.; Zhu, S.L. Hunting for exotic doubly hidden-charm/bottom tetraquark states. *Phys. Lett. B* **2017**, *773*, 247–251. [CrossRef]
61. Chen, W.; Chen, H.X.; Liu, X.; Steele, T.G.; Zhu, S.L. Doubly hidden-charm/bottom $QQ\bar{Q}\bar{Q}$ tetraquark states. *EPJ Web Conf.* **2018**, *182*, 02028. [CrossRef]

62. Wu, J.; Liu, Y.R.; Chen, K.; Liu, X.; Zhu, S.L. Heavy-flavored tetraquark states with the $QQ\bar{Q}\bar{Q}$ configuration. *Phys. Rev. D* **2018**, *97*, 094015. [CrossRef]
63. Debastiani, V.R.; Navarra, F.S. Spectroscopy of the All-Charm Tetraquark. In Proceedings of the XVII International Conference on Hadron Spectroscopy and Structure — PoS(Hadron2017), Salamanca, Spain, 27–29 September 2018; Volume 310, p. 238. [CrossRef]
64. Debastiani, V.R.; Navarra, F.S. A non-relativistic model for the $[cc][\bar{c}\bar{c}]$ tetraquark. *Chinese Phys. C* **2019**, *43*, 013105. [CrossRef]
65. Liu, M.S.; Lü, Q.F.; Zhong, X.H.; Zhao, Q. All-heavy tetraquarks. *Phys. Rev. D* **2019**, *100*, 016006. [CrossRef]
66. Bai, Y.; Lu, S.; Osborne, J. Beauty-full tetraquarks. *Phys. Lett. B* **2019**, *798*, 134930. [CrossRef]
67. Wang, Z.G.; Di, Z.Y. Analysis of the Vector and Axialvector $QQ\bar{Q}\bar{Q}$ Tetraquark States with QCD Sum Rules. *Acta Phys. Polon. B* **2019**, *50*, 1335. [CrossRef]
68. Wang, G.J.; Meng, L.; Zhu, S.L. Spectrum of the fully-heavy tetraquark state $QQ\bar{Q}'\bar{Q}'$. *Phys. Rev. D* **2019**, *100*, 096013. [CrossRef]
69. Bedolla, M.A.; Ferretti, J.; Roberts, C.D.; Santopinto, E. Spectrum of fully-heavy tetraquarks from a diquark+antidiquark perspective. *Eur. Phys. J. C* **2020**, *80*, 1004. [CrossRef]
70. Karliner, M.; Rosner, J.L. Interpretation of structure in the $di-J/\psi$ spectrum. *Phys. Rev. D* **2020**, *102*, 114039. [CrossRef]
71. Lü, Q.F.; Chen, D.Y.; Dong, Y.B. Masses of fully heavy tetraquarks $QQ\bar{Q}\bar{Q}$ in an extended relativized quark model. *Eur. Phys. J. C* **2020**, *80*, 871. [CrossRef]
72. Lundhammar, P.; Ohlsson, T. Nonrelativistic model of tetraquarks and predictions for their masses from fits to charmed and bottom meson data. *Phys. Rev. D* **2020**, *102*, 054018. [CrossRef]
73. Yang, G.; Ping, J.; Segovia, J. Tetra- and Penta-Quark Structures in the Constituent Quark Model. *Symmetry* **2020**, *12*, 1869. [CrossRef]
74. Gordillo, M.C.; De Soto, F.; Segovia, J. Diffusion Monte Carlo calculations of fully-heavy multiquark bound states. *Phys. Rev. D* **2020**, *102*, 114007. [CrossRef]
75. Zhao, J.; Shi, S.; Zhuang, P. Fully-heavy tetraquarks in a strongly interacting medium. *Phys. Rev. D* **2020**, *102*, 114001. [CrossRef]
76. Zhang, J.R. 0^+ fully-charmed tetraquark states. *Phys. Rev. D* **2021**, *103*, 014018. [CrossRef]
77. Obikhod, T.V. Application of the triangulated category to the explanation of fully-charm tetraquark mass. *arXiv* **2021**, arXiv:2103.08449.
78. Wang, Z.G. Revisit the tetraquark candidates in the $J/\psi J/\psi$ mass spectrum. *Int. J. Mod. Phys. A* **2021**, *36*, 2150014. [CrossRef]
79. Li, Q.; Chang, C.H.; Wang, G.L.; Wang, T. Mass spectra and wave functions of $T_{QQ\bar{Q}\bar{Q}}$ tetraquarks. *Phys. Rev. D* **2021**, *104*, 014018. [CrossRef]
80. Nefediev, A.V. $X(6200)$ as a compact tetraquark in the QCD string model. *Eur. Phys. J. C* **2021**, *81*, 692. [CrossRef]
81. Yang, B.C.; Tang, L.; Qiao, C.F. Scalar fully-heavy tetraquark states $QQ'\bar{Q}\bar{Q}'$ in QCD sum rules. *Eur. Phys. J. C* **2021**, *81*, 324. [CrossRef]
82. Weng, X.Z.; Chen, X.L.; Deng, W.Z.; Zhu, S.L. Systematics of fully heavy tetraquarks. *Phys. Rev. D* **2021**, *103*, 034001. [CrossRef]
83. Tiwari, R.; Rathaud, D.P.; Rai, A.K. Spectroscopy of all charm tetraquark states. *Indian J. Phys.* **2022**. [CrossRef]
84. Wang, G.J.; Meng, L.; Oka, M.; Zhu, S.L. Higher fully charmed tetraquarks: Radial excitations and P-wave states. *Phys. Rev. D* **2021**, *104*, 036016. [CrossRef]
85. Zhao, Z.; Xu, K.; Kaewsnod, A.; Liu, X.; Limphirat, A.; Yan, Y. Study of charmoniumlike and fully-charm tetraquark spectroscopy. *Phys. Rev. D* **2021**, *103*, 116027. [CrossRef]
86. Lesteiro-Tejeda, J.A.; Ramírez-Zaldívar, D.A.; Gracía-Trápaga, C.E.; Guzmán-Martínez, F. Spectroscopy of the tetraquark $c\bar{c}-c\bar{c}$ in a non-relativistic approach using a phenomenological QCD model. *arXiv* **2021**, arXiv:2101.03192.
87. Mutuk, H. Nonrelativistic treatment of fully-heavy tetraquarks as diquark-antidiquark states. *Eur. Phys. J. C* **2021**, *81*, 367. [CrossRef]
88. Wang, Q.N.; Yang, Z.Y.; Chen, W. Exotic fully heavy $QQ\bar{Q}\bar{Q}$ tetraquark states in $\mathbf{8}_{[Q\bar{Q}]} \otimes \mathbf{8}_{[Q\bar{Q}]}$ color configuration. *Phys. Rev. D* **2021**, *104*, 114037. [CrossRef]
89. Ke, H.W.; Han, X.; Liu, X.H.; Shi, Y.L. Tetraquark state $X(6900)$ and the interaction between diquark and antidiquark. *Eur. Phys. J. C* **2021**, *81*, 427. [CrossRef]
90. Zhu, R. Fully-heavy tetraquark spectra and production at hadron colliders. *Nucl. Phys. B* **2021**, *966*, 115393. [CrossRef]
91. Kuang, Z.; Serafin, K.; Zhao, X.; Vary, J.P. All-charm tetraquark in front form dynamics. *Phys. Rev. D* **2022**, *105*, 094028. [CrossRef]
92. Majarshin, A.J.; Luo, Y.A.; Pan, F.; Segovia, J. Bosonic algebraic approach applied to the $[QQ][\bar{Q}\bar{Q}]$ tetraquarks. *Phys. Rev. D* **2022**, *105*, 054024. [CrossRef]
93. Wang, Z.G. Analysis of the $X(6600)$, $X(6900)$, $X(7300)$ and related tetraquark states with the QCD sum rules. *arXiv* **2022**, arXiv:2207.08059.
94. Wang, G.J.; Meng, Q.; Oka, M. The S-wave fully-charmed tetraquark resonant states. *arXiv* **2022**, arXiv:2208.07292.
95. An, H.T.; Luo, S.Q.; Liu, Z.W.; Liu, X. Systematic search of fully heavy tetraquark states. empharXiv **2022**, arXiv:2208.03899.
96. Zhuang, Z.; Zhang, Y.; Ma, Y.; Wang, Q. Lineshape of the compact fully heavy tetraquark. *Phys. Rev. D* **2022**, *105*, 054026. [CrossRef]
97. Chao, K.T. The $(cc)-(\bar{c}\bar{c})$ (Diquark - Antidiquark) States in e^+e^- Annihilation. *Z. Phys. C* **1981**, *7*, 317. [CrossRef]
98. Chiu, T.W.; Hsieh, T.H. $Y(4260)$ on the lattice. *Phys. Rev. D* **2006**, *73*, 094510. [CrossRef]
99. Wang, Z.G. Tetraquark candidates in LHCb's $di-J/\psi$ mass spectrum. *Chinese Phys. C* **2020**, *44*, 113106. [CrossRef]

100. Liu, F.X.; Liu, M.S.; Zhong, X.H.; Zhao, Q. Higher mass spectra of the fully-charmed and fully-bottom tetraquarks. *Phys. Rev. D* **2021**, *104*, 116029. [CrossRef]
101. Chen, X. Fully-heavy tetraquarks: $bb\bar{c}\bar{c}$ and $bc\bar{b}\bar{c}$. *Phys. Rev. D* **2019**, *100*, 094009. [CrossRef]
102. Yang, Z.Y.; Wang, Q.N.; Chen, W.; Chen, H.X. Investigation of the stability for fully-heavy $bc\bar{b}\bar{c}$ tetraquark states. *Phys. Rev. D* **2021**, *104*, 014003. [CrossRef]
103. Esposito, A.; Polosa, A.D. A $bb\bar{b}\bar{b}$ di-bottomonium at the LHC? *Eur. Phys. J. C* **2018**, *78*, 782. [CrossRef]
104. Vogt, R.; Angerami, A. Bottom tetraquark production at RHIC? *Phys. Rev. D* **2021**, *104*, 094025. [CrossRef]
105. Tiwari, R.; Rathaud, D.P.; Rai, A.K. Mass-spectroscopy of $[bb][\bar{b}\bar{b}]$ and $[bq][\bar{b}\bar{q}]$ tetraquark states in a diquark–antidiquark formalism. *Eur. Phys. J. A* **2021**, *57*. [CrossRef]